

PHASE TRANSFORMATIONS IN HETEROGENEOUS STEELS

by

Shahid Amin Khan

*Wolfson College*

*Cambridge*

A dissertation submitted for the fulfilment  
of the Degree of Doctor of Philosophy  
at the University of Cambridge

*February 1990*

---

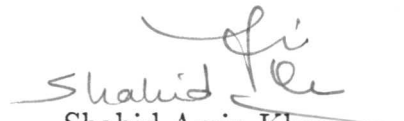
- A first rate theory predicts; a second rate theory forbids, and a third rate theory explains after the event.

*A. I. Kitaigorodskii*, Quoted A. L. Mackay,  
"Harvest of A Quiet Eye"

★ *To the present, past and future inhabitants of "Bait-ul-Amin".....my home.*

## PREFACE

This dissertation, which is submitted for the degree of Doctor of Philosophy in the University of Cambridge, describes research carried out under the supervision of Dr. H. K. D. H. Bhadeshia in the Department of Materials Science and Metallurgy, Cambridge, between April 1986 and January 1990. Except where acknowledgement, and reference to previous work has been made, this work is, to my best knowledge, original and has been done without collaboration. Neither this dissertation, nor any one substantially similar to it has been or is being submitted for a degree, diploma or other qualification at any other University. This dissertation consists of less than sixty thousand words.

  
Shahid Amin Khan,

February, 1990.

## ACKNOWLEDGEMENT

I feel great pleasure in expressing my heartiest obligations to Dr. H. K. D. H. Bhadeshia for his continued guidance, encouragement and support at every turning and Professor D. Hull for the provision of laboratory facilities at the University of Cambridge. I am also grateful to my present and past colleagues in the Phase Transformations group, in particular Dr. J-R. Yang ( To whom special thanks are also due), Dr. S. Atamert, Mr. A. Ali and Mr. S. Babu.

I greatly acknowledge my family and the friends back home for their constant support during the period of my research. A very special thanks goes to Mr. Ali's family, in Cambridge, for providing me with shelter and food during the crucial days of my thesis. Mr. M. Ikram (Cavendish Laboratory) and Mr. S. A. Mujahid should also be acknowledged for taking me through some of the difficult mathematical steps.

Thanks are also extended to the technical staff of the Department, particularly Mr. J. Leader, Mr. D. A. Nickol, Mrs. K. Butler, Mr. B. Barber and Mr. G. Morgan for their technical help.

This work is supported by the Ministry of Science and Technology, Government of Pakistan, to whom acknowledgement is also made.

Last but not least, let me acknowledge my patience to see the thesis in this form.

## CONTENTS

PREFACE .....	i
ACKNOWLEDGEMENT .....	ii
CONTENTS .....	iii
CHAPTER ONE	
<u>SOME ASPECTS OF PHASE TRANSFORMATIONS</u>	
1.1 Introduction .....	1
1.2 Liquid to solid transformation .....	1
1.3 Decomposition of austenite .....	2
1.4 Role of alloying elements in transformation kinetics .....	11
1.5 Prediction of microstructure .....	14
References .....	22
CHAPTER TWO	
<u>HETEROGENEITY AND PHASE TRANSFORMATIONS</u>	
2.1 Introduction .....	25
2.2 Chemical heterogeneity .....	25
2.3 Homogenization .....	39
2.4 Segregation and properties of materials .....	41
2.5 Heterogeneity and phase transformations .....	45
References .....	57
CHAPTER THREE	
<u>EXPERIMENTAL TECHNIQUE</u>	
3.1 Materials .....	59
3.2 Heat-treatment .....	59
3.3 Optical microscopy .....	60
3.4 Dilatometry .....	60
3.5 Microhardness testing .....	61
3.6 Microanalysis .....	61

3.7 Transmission electron microscopy .....	61
--------------------------------------------	----

## CHAPTER FOUR

### THE BAINITE TRANSFORMATION IN CHEMICALLY HETEROGENEOUS 300M HIGH – STRENGTH STEEL

4.1 Introduction .....	62
4.2 Results and Discussion .....	64
4.3 Conclusions .....	73
References .....	98

## CHAPTER FIVE

### KINETICS OF MARTENSITIC TRANSFORMATION IN PARTIALLY BAINITIC 300M STEEL

5.1 Introduction .....	100
5.2 Dilatometry .....	101
5.3 Kinetics of athermal martensitic transformation .....	105
5.4 Conclusions .....	111
References .....	124

## CHAPTER SIX

### REAUSTENITISATION IN HETEROGENEOUS STEELS

6.1 Introduction .....	127
6.2 Isothermal reaustenitisation .....	128
6.3 Results and discussion .....	130
6.4 Conclusions .....	135
References .....	161

## CHAPTER SEVEN

### ALLOTRIOMORPHIC FERRITE FORMATION IN A HETEROGENEOUS STEEL

7.1 Introduction .....	163
7.2 Theoretical Analysis .....	163
7.3 Dilatometry .....	168
7.4 Conclusions .....	170

References .....190

CHAPTER EIGHT

COMPLETE CALCULATION OF MICROSTRUCTURAL EVOLUTION IN  
HETEROGENEOUS AUTOMOBILE STEELS

8.1 Introduction ..... 191  
8.2 Dilatometry .....191  
8.3 Transformation to bainitic ferrite ..... 194  
8.4 Martensitic transformation in ‘US83’ steel ..... 196  
8.5 Conclusions ..... 197  
References ..... 229

CHAPTER NINE

SUMMARY AND FURTHER WORK

9.1 Summary ..... 230  
9.2 Further work ..... 231  
  
APPENDIX 1 ..... 232  
APPENDIX 2 ..... 242  
APPENDIX 3 ..... 251  
APPENDIX 4 ..... 257  
APPENDIX 5 ..... 263  
APPENDIX 6 ..... 265

## Chapter 1

# SOME ASPECTS OF PHASE TRANSFORMATIONS IN STEELS

### 1.1 Introduction

It is the primary aim of the present work to investigate the effect of chemical segregation in austenite on its transformation to different phases. These phases may vary not just in morphology, but in transformation mechanisms, phase compositions, crystallographic structure and thermodynamic stability. This literature survey is intended to describe the morphologies of different microstructures and to summarise their transformation mechanisms where they are known.

Castings and weld deposits both usually experience three major transformations during the course of their manufacture:

- (1) liquid to solid transformation, with the product phase being either primary austenite ( $\gamma$ ) or delta ferrite ( $\delta$ );
- (2) transformation of delta ferrite to austenite if this is not the primary solidification phase;
- (3) further decomposition of austenite to a variety of transformation products such as allotriomorphic ferrite, Widmanstätten ferrite, bainitic ferrite and martensite.

The chemical segregation of substitutional solutes can occur on a relatively major scale during transformations (1) and (2), but this can subsequently influence the transformations described in (3).

### 1.2 Liquid to Solid Transformation

The fundamental principles of the solidification of cast metals are now very well understood<sup>[1,2]</sup> and attempts have been made to apply<sup>[3,4]</sup> them to the study of weld pool solidification. The situation in welding is more complicated due to the movement of the heat source so that melting, mixing and freezing occur at different points within the same pool and the direction of maximum heat flow varies with time during solidification, so that the simplified one dimensional approximations valid for ingot solidification do not always hold for welding situation. It is intended to present here a brief comparison of ingot and weld pool solidification.

- Nucleation, particularly, heterogeneous nucleation is the norm in ingot solidification and the formation of chill, columnar and equiaxed microstructure is observed. In weld pool solidification no nucleation stage is involved and continuity of grains exists across the HAZ/fusion zone interface<sup>[5,6]</sup>.
- The absence of equiaxed microstructure in welds is due to the very severe thermal conditions in the melt. Generally the weld pool volume is small compared with the surrounding components, which act as a huge heat sink, and, along with low heat input give rise to very large thermal gradients, rapid cooling and hence stresses. A reasonably constant thermal gradient exists during ingot solidification.
- Only slight turbulence is experienced by an ingot depending on pouring conditions but electromagnetic stirring of the weld pool generated by Lorentz forces create conditions of considerable turbulence with in the pool<sup>[7]</sup>.

### 1.3 Decomposition of Austenite

When austenite is rapidly cooled to a very low temperature, there may not be enough time or atomic mobility to facilitate the reconstructive formation of ferrite. Under this circumstances, Widmanstätten ferrite, bainite or martensite can be produced depending on the level of the undercooling. In contrast, when specimens are cooled to relatively high temperature below  $A_{e3}$ , the austenite phase can undergo complete reconstruction into the ferrite phase. The key characteristics of phase transformations in steels have been summarised by Bhadeshia<sup>[8]</sup>

#### 1.3.1 Allotriomorphic Ferrite

The layer like shape of this phase is such that it does not reflect the symmetry of its crystal structure. The other terms such as grain boundary ferrite, polygonal ferrite and proeutectoid ferrite are too general and fail to distinguish between Widmanstätten ferrite and allotriomorphic ferrite, both of which can form above the eutectoid temperature and at austenite grain boundaries.

The allotriomorphic ferrite usually nucleates at the austenite grain boundaries. The classical view<sup>[9,10]</sup> is that transformation occurs with  $\alpha$  nuclei forming a partially coherent interface with atleast one of the adjacent austenite grains, while a random relation exists with the other. The partially coherent interface is then believed to move

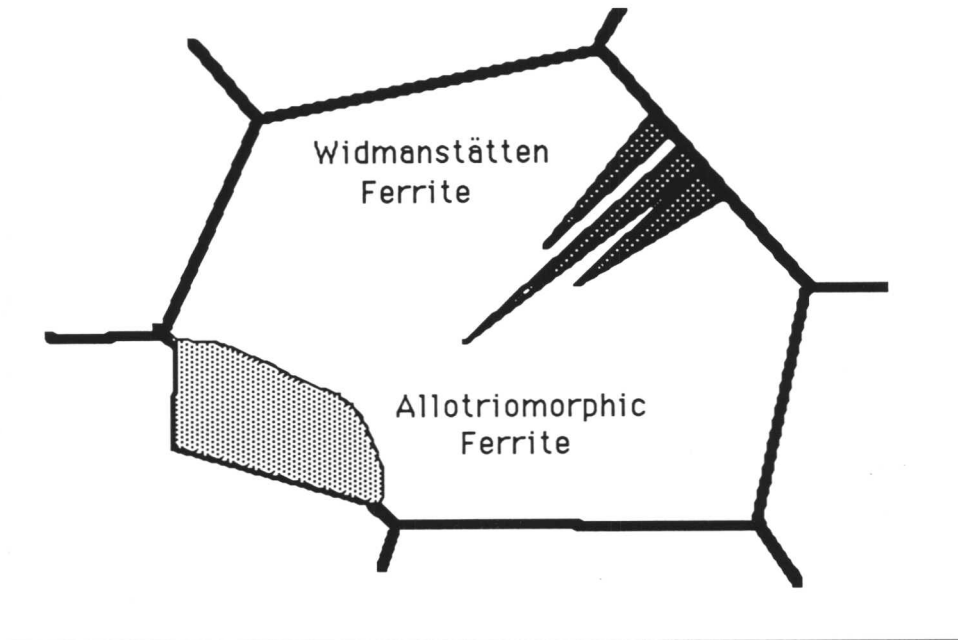


**Fig. 1.1:** Schematic representation of the grain boundary nucleation of allotriomorphic ferrite and Widmanstätten ferrite.

by the displacement of ledges; while the other relatively high energy interface is supposed to be displaced by the continuous motion of the whole interface in a direction normal to itself. According to Hillert<sup>[11]</sup>, a ferrite nucleus can have rational orientation relationships with both the adjacent austenite grains in some cases if crystallographic texture in the austenite permits it. Further growth is usually extremely rapid in low-alloy steels, with the allotriomorphic ferrite forming almost continuous layers along the  $\gamma$  grain boundaries as shown in Fig. 1.1. The kinetics of growth of allotriomorphic ferrite are very important to models of microstructure prediction, as the fraction of ferrite determines the volume fraction of austenite available to subsequently form the other phases and also the degree of carbon enrichment of the remaining austenite. Allotriomorphic ferrite is perceived as being detrimental to the toughness. Its continuous layer morphology provides minimal resistance to crack propagation<sup>[12,13]</sup>.

### 1.3.2 Widmanstätten Ferrite

Widmanstätten ferrite forms in a temperature range where reconstructive transformation becomes relatively sluggish and gives way to displacive transformations. It has the shape of a thin wedge (Fig. 1.2), the actual shape being somewhere between that of a plate and a lath<sup>♣</sup>. The displacive transformation mechanism should cause the generation of a large strain energy, incompatible<sup>[14]</sup> with the low undercooling below the  $A_{e3}$  temperature where  $\alpha_W$  forms, but is largely eliminated by the simultaneous formation of two back-to-back self accommodating plates, as shown in Fig. 1.2, whose shear displacements cancel to a large extent. The characteristic wedge shape is a consequence of the slight misorientation of the habit planes of these two variants. Both the adjacent variants of Widmanstätten ferrite plates have been known to possess a Kurdjumov-Sachs type orientation relation with the parent austenite<sup>[15]</sup>.

Because  $\alpha_W$  forms at lower undercoolings, the diffusion of carbon during growth is a thermodynamic necessity. However, the growth rate of Widmanstätten ferrite ( $\alpha_W$ ) is higher than would be expected from the diffusion controlled motion of carbon planar interface because multidirectional diffusion occurs at the tip compared with unidirectional diffusion ahead of a plane boundary as shown in Fig. 1.3. The displacive nature of this product means that the effect of alloying elements such as Mn, Ni and Cr is less than for allotriomorphic ferrite. At high alloying levels the temperature at which  $\alpha_W$  can form is depressed so much that the undercooling is high enough for bainite formation, which occurs at the expense of  $\alpha_W$ . Thus  $\alpha_W$  will not form as a distinguishable phase ( $W_s=B_s$ ). Again elements such as Mo, which for unexplained reasons, remove grain boundary nucleation sites will reduce the amount of  $\alpha_W$  form in a similar way to allotriomorphic ferrite ( $\alpha_a$ ).

Boron, which has a strong retarding effect upon the nucleation of allotriomorphic ferrite ( $\alpha_a$ ) has a negligible effect upon displacive transformation products and would not be expected to retard formation of  $\alpha_W$ . Widmanstätten ferrite is an undesirable constituent because of its inferior toughness properties<sup>[16,17]</sup>.

---

<sup>♣</sup> *If a plate or lath is idealised as a rectangular parallelepiped with sides of lengths  $a$ ,  $b$ , and  $c$ , then  $a=b \gg c$  for a plate and  $a \gg b \gg c$  for a lath.*

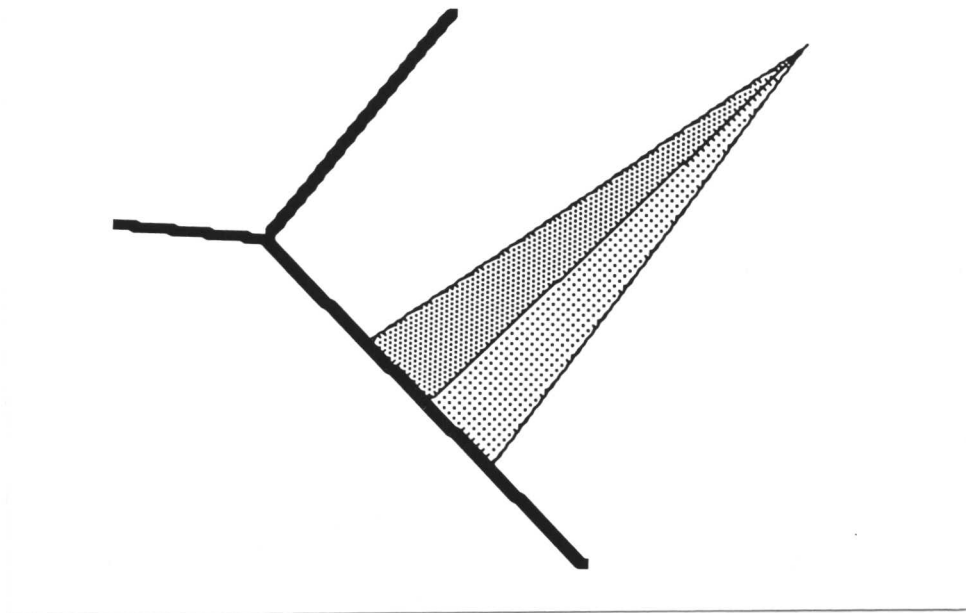


**Fig. 1.2:** *The back-to-back growth of Widmanstätten ferrite plates in order to mutually accommodate their shear displacements.*

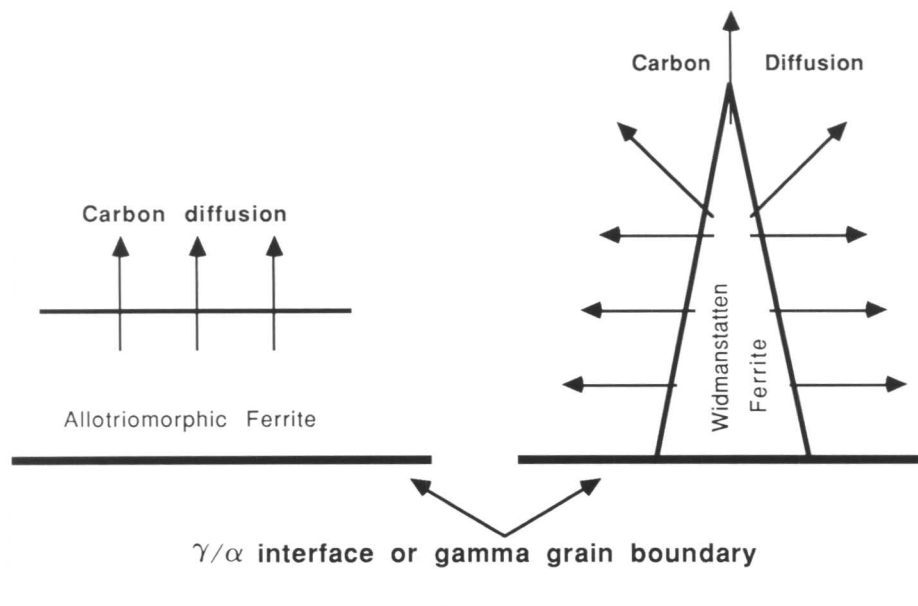


**Fig. 1.3:** *Multidirectional diffusion in case of Widmanstätten ferrite as compared with diffusion just ahead of the interface in case of allotriomorphic ferrite growth.*

### 1.3.3 The Bainite Transformation

Bainite, another product of a displacive reaction, is a non-lamellar aggregate of plate-shaped ferrite and carbides. However, in some cases carbides may be totally absent<sup>[18]</sup> *e.g.* , upper bainite in Si steels. The bainite transformation has been summarised by Christian and Edmonds<sup>[19]</sup> and more recently by Bhadeshia and Christian<sup>[20]</sup>. It is concluded that the incoherent ledge mechanism of growth, as proposed by Aaronson *et al.* <sup>[21]</sup>, is not probable for bainite. Furthermore, it is now established that the transformation can only occur at a certain degree of undercooling below the  $T_0$  temperature<sup>\*</sup>. The undercooling required is lower than that associated with the athermal martensite transformation, primarily due to the lower stored energy of bainite, and because of specific differences in nucleation behaviour, *i.e.*, the nucleation of bainite does involve the partitioning of carbon<sup>[22]</sup> whereas for martensite both nucleation and growth are diffusionless.

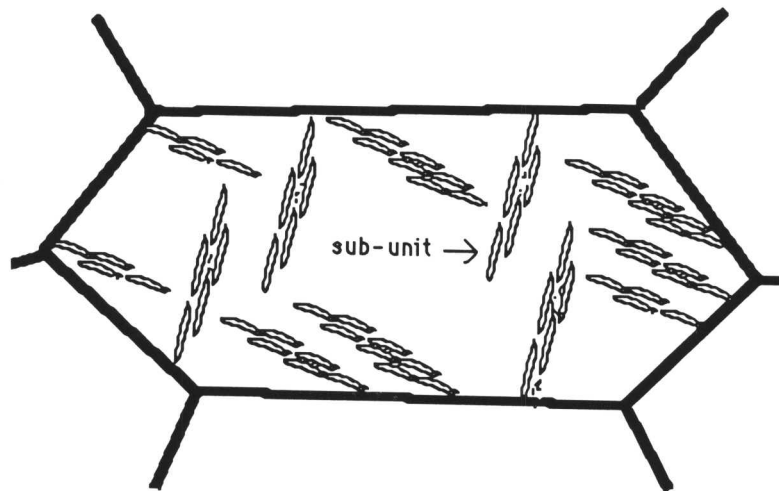


Fig. 1.4: The morphology of bainite as it nucleates at prior austenite grain boundaries, and then autocatalytic nucleation of sub-units result in the formation of a sheaf. It should be noted that sub-units are continuous.

\* The  $T_0$  temperature refers to a temperature at which ferrite ( $\alpha$ ) and austenite ( $\gamma$ ) of identical composition have the same free energy.

Bainite grows by a diffusionless mechanism, but because of the relatively high temperatures at which it occurs, the excess carbon is either rapidly rejected into the remaining austenite or precipitates in the form of carbides in the ferrite. The relatively low driving force at the  $B_s$  temperature leads to a limited sub-unit size, (Fig. 1.4) the limitation coming into force when the chemical free energy change can no longer drive the transformation interface through the myriad of accommodation defects that are found to accompany the formation of bainite. The isothermal character of bainite transformation arises since new subunits can only nucleate autocatalytically when the carbon concentration in the vicinity of the prior subunit (*i.e.*, the carbon build-up resulting from post-bainitic partitioning) is reduced by diffusion to a sufficiently low level such that displacive transformation is thermodynamically allowed. At a certain degree of transformation (depending on temperature and alloy composition), the carbon content of the austenite will reach a level such that the  $T_0$  condition is transgressed, and displacive transformation then ceases. This is the incomplete reaction phenomenon, the term incomplete referring to the fact that the reaction stops well before the carbon content of the austenite reaches the level specified by the  $\alpha + \gamma/\gamma$  equilibrium or paraequilibrium phase boundaries. Direct observations (at atomic resolution) have shown<sup>[23]</sup> that segregation induced solute drag cannot be claimed to influence the growth of bainite. The bainite bay in alloy steels is probably due to the overlapping of separate C-curves for the different reactions rather than to solute drag on a ferrite-austenite interface. The observed shape change implies an atomic correspondence during growth, the necessity for which arises from the low mobility of the iron atoms at the transformation temperatures.

There are two classical morphologies of bainite.

#### 1.3.3.1 Upper Bainite

This consists of platelets of ferrite adjacent to each other, and in very nearly the same crystallographic orientation in space, so that wherever two adjacent platelets touch, a low angle boundary arises. Elongated cementite particles usually decorate the boundaries of these platelets, the amount and continuity of these slabs of cementite depending on the carbon content of the steel. The ferrite platelets, which form a sheaf, have the same habit plane, and the sheaf itself has a thin wedge plate morphology in three dimensions. The slabs of cementite actually form from the austenite between the

ferrite platelets, and hence do not have a reproducible orientation relation with the  $\alpha$  since they precipitate from austenite. Fig. 1.5 illustrates schematically the transition from upper bainite to lower bainite.

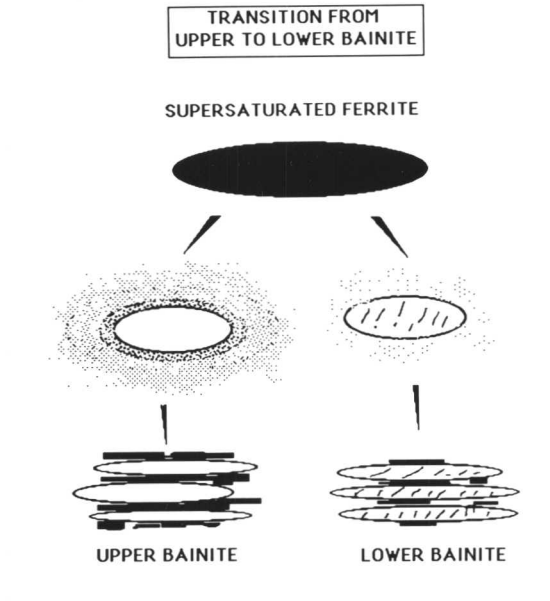


**Fig. 1.5:** When the time to decarburise the ferrite is small relative to that required to relieve the carbon supersaturation by the precipitation of carbides within the ferrite, then upper bainite is obtained; otherwise, lower bainite forms<sup>[24]</sup>.

### 1.3.3.2 Lower Bainite

This is basically very similar to upper bainite, except that the amount of interplate cementite is less, and carbides can be found within the ferrite itself. These intra-ferrite carbides can be epsilon carbide (in high-carbon or medium carbon silicon steels) or cementite plates precipitated in a single crystallographic orientation with respect to  $\alpha$ , with the habit plane inclined at about  $60^\circ$  to the plate axis. There are however cases where more than one variant can be observed<sup>[25,26]</sup>.

The orientation relationship between bainitic ferrite and austenite is close to either the Kurdjumov-Sachs or the Nishiyama-Wasserman orientation. The ferrite and cementite are relatively oriented by a variant of the Bagaryatskii relationship commonly observed for the precipitation of cementite in tempered martensite, or other kinds of tempering orientation relationships.

### 1.3.4 Acicular Ferrite

Acicular ferrite appears as a fine grained interlocking array of non-parallel laths. Recent work<sup>[27,28]</sup> has shown that acicular ferrite is in fact intragranularly nucleated bainite. It differs morphologically from classical sheaf-like bainite firstly because it nucleates intragranularly, either on inclusions, or sympathetically on pre-existing plates, secondly because growth is limited by physical impingement with other plates which form on neighbouring sites. This is shown schematically in Fig. 1.6. Acicular ferrite requires the presence of inclusions to enable intragranular nucleation and will only form when the austenite grain size is relatively large, so that events originated from the grain boundaries do not swamp those occurring intragranularly. Intragranular nucleation on inclusions has a higher activation energy when compared with grain boundary nucleation<sup>[29]</sup> so that the number of grain boundary nucleation sites must be minimised to obtain acicular ferrite.

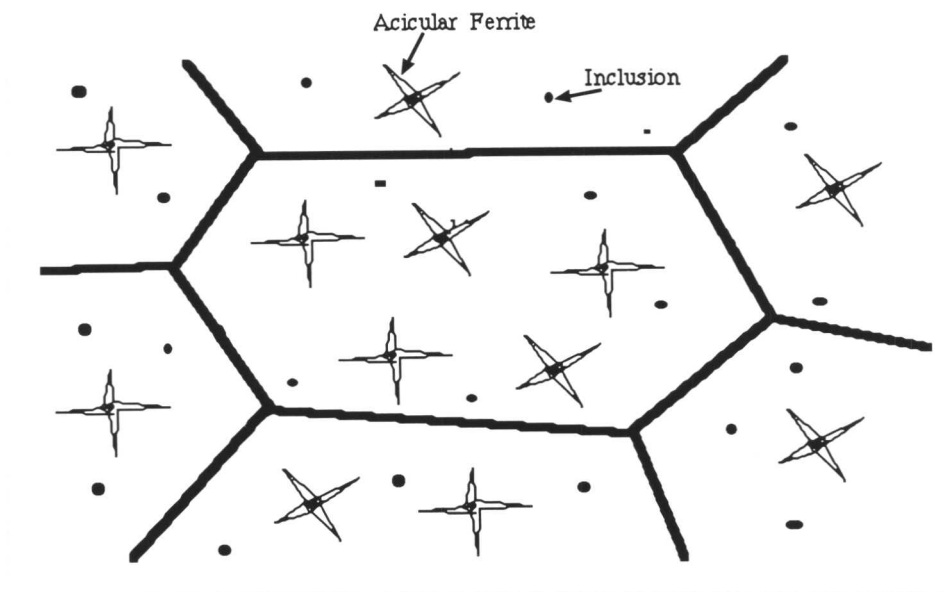


**Fig. 1.6:** Randomly placed acicular ferrite nucleates on the inclusions and is just another variant of bainite which nucleates at prior austenite grain boundaries and exhibits aligned morphology.

Acicular ferrite is a highly desirable constituent in steel welds due to its fine grain size and interlocking nature, often referred to “basket weave structure”<sup>[30]</sup>. The large number of non-parallel grain boundaries hinder crack propagation and the impact toughness is thus improved<sup>[31–33]</sup>.

### 1.3.5 Martensitic Transformation

Martensitic transformations are a subclass of displacive, diffusionless, and first-order phase transformations in which the kinetics and morphology are dominated by the strain energy arising from shear-like displacements. The transformation kinetics are controlled by the nucleation rate and not by the growth rate because the growth rate is relatively fast. A necessary condition for the occurrence of martensitic transformation is that the free energy of martensite should be lower than that of austenite. Moreover, since additional energy, such as that due to surface energy and transformation strain energy, is necessary for the transformation to take place, the difference between the free energies of austenite and martensite must exceed the required additional energy. Therefore the austenite to martensite transformation cannot occur until the specimen is cooled to a particular temperature below the value where the free energy difference between austenite and martensite is zero. This temperature is called martensitic transformation start temperature ( $M_s$ ). The overall kinetics of martensitic reactions is greatly influenced by autocatalytic nucleation<sup>[34]</sup>, but the phenomena have received relatively little systematic study so far. Martensitic transformation kinetics in steels are either athermal or isothermal.

#### 1.3.5.1 Autocatalytic Nucleation

The preexisting sites are not enough to account for all the martensitic units observed. These excess sites are generally attributed to autocatalysis. Three mechanisms<sup>[35]</sup> have been proposed for autocatalysis, relying on the fact that immediate vicinity of a plate is disturbed quite severely by a combination of elastic and plastic deformation processes due to the shear like nature of the transformation.

- *Stress-induced Nucleation, i.e.*, the activation of less potent defects at a given temperature by the internally generated elastic stresses.
- *Strain-induced Nucleation, i.e.*, the creation of new and more potent nucleating defects by the dislocation generation and rearrangement during plastic accommodation of the parent phase in response to the transformational shape change.
- *Interfacial Autocatalysis, i.e.*, direct nucleation of new martensitic units from the existing martensitic interfacial dislocations by a secondary dissociation process.

## 1.4 Role Of Alloying Elements in Transformation Kinetics Steels

The aim of this section is to mention briefly how alloy additions influence transformations in steels. Specific effects are dealt with in detail as they arise in the text. The effect of alloy elements in steels is twofold. They can affect both the thermodynamics and kinetics of transformations. The hardenability of steels is related directly to the influence on the nucleation and growth kinetics of the decomposition products. Primarily, hardenability of steels is defined in terms of the mean depth and distribution of martensite in specimens quenched under standard conditions. The ability to form martensite is dependent, in turn, on the ability to suppress (partially or completely) the formation of other austenite decomposition products such as allotriomorphic ferrite and cementite, pearlite, and bainite. For a given steel, a useful index of the ability to suppress the reconstructive transformation of austenite is the location of the nose (or noses) on the corresponding time-temperature-transformation (TTT) curve. Recognising that this location is determined by the nucleation and growth kinetics of the decomposition products, it is important to consider the influence of alloying elements on the kinetics of reaction.

The effect of alloying elements on the transformation of austenite<sup>[36-41]</sup> has been studied considering the behaviour of an alloying element in and close to the moving interface. The rate at which an interface moves depends both on its intrinsic mobility (*i.e.*, related to the process of atom transfer across the interface) and on the ease with which any alloying element partitioned during transformation diffuses ahead of the interface<sup>[15]</sup>. Both of these processes dissipate the free energy ( $\Delta G$ ) available for interface motion; when  $\Delta G$  is mainly used up in driving the diffusion of solute ahead of the interface, growth is said to be diffusion-controlled. On the other hand, interface-controlled growth occurs when most of  $\Delta G$  is dissipated in the process of atom transfer across the interface. In Fe-X-C ternary systems (where X is a substitutional alloying element), the diffusion-controlled growth is complicated by the fact that both interstitial and substitutional atomic diffusion occurs during transformation. Substantial differences in the diffusion coefficients of the interstitial and substitutional elements along with the assumption of local equilibrium at the interface leads to a variety of possible growth modes<sup>[36-41]</sup>.

#### 1.4.1 Partitioning Local Equilibrium (P-LE)

For low supersaturations, X (the substitutional solute) partitions between the daughter ( $\alpha$ ) and parent ( $\gamma$ ) phases. The flux of C is reduced by making the C-concentration gradient very shallow (Fig. 1.7a). The precipitate growth rate is low and is determined by the slow diffuser X *i.e.*, X exerts a diffusional drag on the growth kinetics, which is consequence of the fact that it diffuses many orders of magnitude slower than carbon.

#### 1.4.2 Negligible Partitioning Local Equilibrium (NP-LE)

For rather high supersaturations, the precipitate growth rate is relatively high and is determined by the fast diffuser, C. In this regime, X, exerts essentially no diffusional drag effect, in spite of its low diffusivity. The gradient of X is made very steep to increase flux (Fig. 1.7b), by partitioning very little X from  $\gamma$  to  $\alpha$ . As supersaturation is changed by alloying element additions, both nucleation and growth should be influenced in the same way, *i.e.*, accelerated for increased supersaturations, and retarded for decreased supersaturations.

A given bulk composition is expected to pass from NP-LE to P-LE regime with increasing temperature. During NP-LE growth the width of the X concentration spike in  $\gamma$  can be a few nm. As the temperature of transformation decreases, the X concentration spike also decreases until it becomes approximately equal to atomic dimensions. It is usually assumed that the condition is then reached where the substitutional atoms become configurationally frozen, and equilibrium breaks down at interface. This constrained equilibrium, in which X is not redistributed during transformations, is known<sup>[42]</sup> as “paraequilibrium”. However, C is still mobile, and subject to the constraint that Fe/X ratio is identical in  $\alpha$  and  $\gamma$ , it reaches “equilibrium”. It is currently not possible to decide theoretically which of these modes is favoured in a particular set of circumstances, and experimental evidence does not help since it is not in general sufficiently precise. The possible existence of solute drag effects and interface pinning effects may further complicate the interpretation of experimental evidence. All these effects are expected to be more complicated in the case of segregated steels.

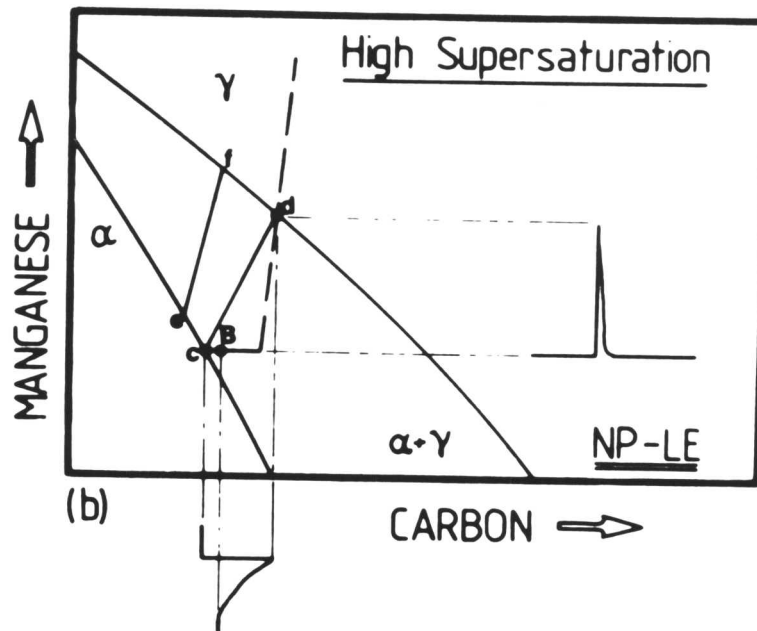
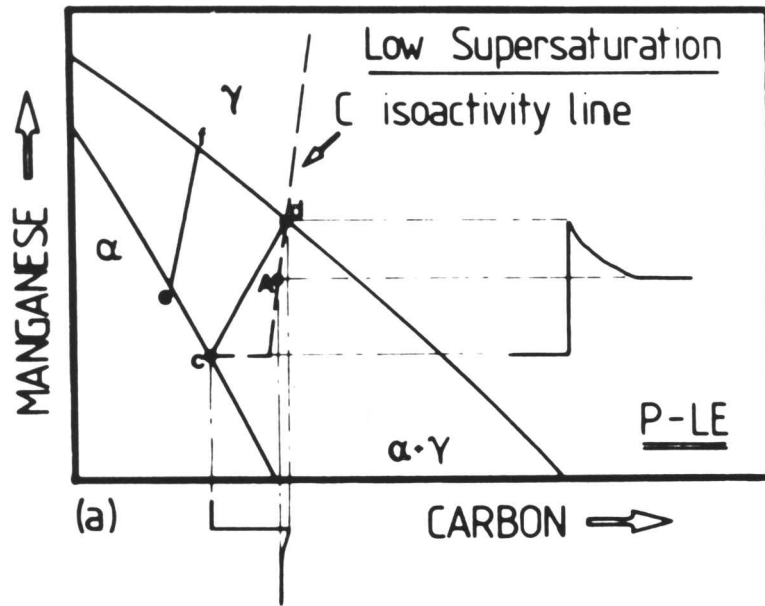
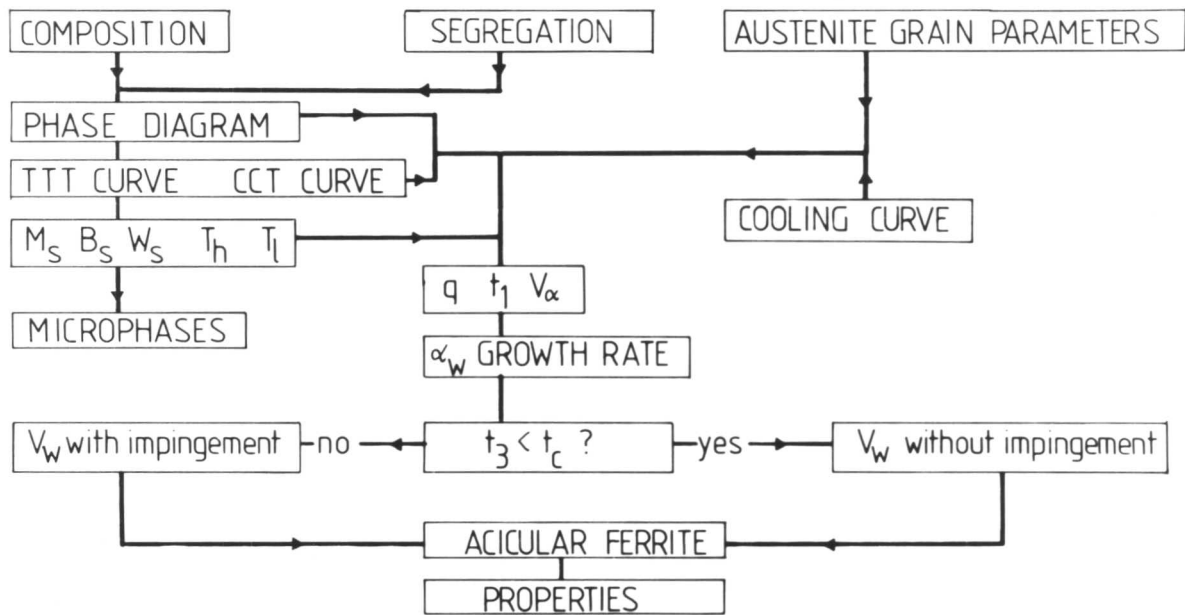


Fig. 1.7: If local equilibrium is maintained at the  $\alpha/\gamma$  interface, two modes of allotriomorphic ferrite growth in Fe-C-X (where X is a substitutional alloying element) are possible, depending on the alloy composition. These modes are shown in the above diagrams, where X is Mn (after Bhadeshia<sup>[15]</sup>). (a) Growth at low supersaturations (P-LE) with bulk redistribution of Mn, (b) growth at high supersaturations (NP-LE) with negligible partitioning of Mn during transformation.

## 1.5 Prediction of Microstructure

Bhadeshia *et al.*,<sup>[43-47]</sup> have developed a model to predict the microstructure in low alloy welds using the phase transformation theory outlined in the previous sections and can be applied to wrought steels. The steps involved in the calculations of microstructure in this model are represented in a flow chart (Fig. 1.8).



**Fig. 1.8:** Flow chart illustrating the steps involved in the calculation of the microstructure.  $T_h$  is the high temperature at which allotriomorphic ferrite ( $V_\alpha$  in the diagram) starts forming.  $q$  is the half thickness of allotriomorphic ferrite layer.  $T_l$  is the temperature below which displacive transformations are assumed to be kinetically favoured and is obtained by the cross-over point of the two C curves.  $t_1$  is the time taken for the weld deposit to cool from  $T_h$  temperature to  $T_l$  temperature.  $t_3$  is the time available for Widmanstätten ferrite to grow right across the austenite grains.  $t_c$  is the critical time before an impingement occurs (after Bhadeshia *et al.* [48]).

To start with austenite grains are assumed to have a morphology of hexagonal prisms as illustrated in Fig. 1.9. An estimation of solute segregation during solidification (assumed to be equilibrium) is made on the basis of their segregation tendencies. From the knowledge of chemical composition, austenite grain size parameters and

cooling curve, phase diagrams and time-temperature-transformation (TTT) curves are calculated for solute-enriched and solute-depleted regions. The model assumes all the alloying elements to be in solid solution and is valid for up to 5 wt.% of total alloying additions.

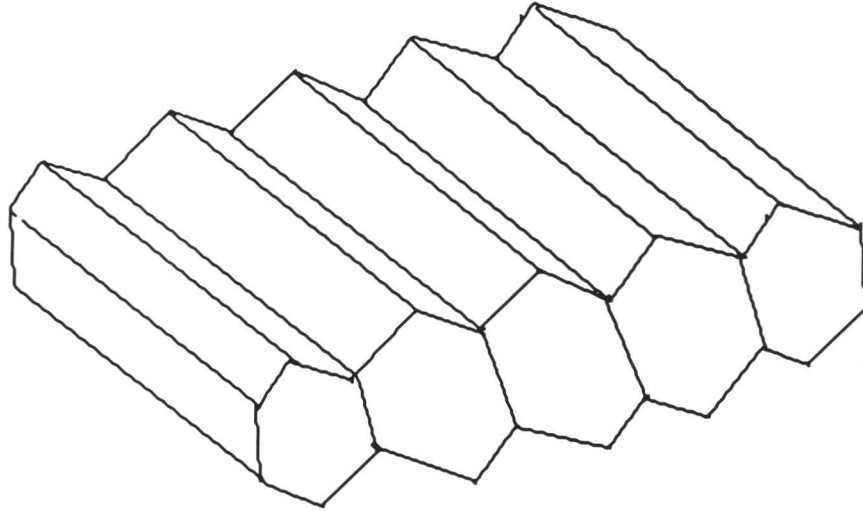


**Fig. 1.9:** For the purpose of modelling the austenite grains are approximated as space filling hexagonal prisms.

### 1.5.1 Isothermal Transformation Diagrams

Bhadeshia's empirical model to generate the time-temperature-transformation (TTT) diagrams for the alloy steels, containing C, Mn, Si, Ni, Cr, Mo and V is formally based on Russell's equation<sup>[49]</sup> for incubation time<sup>♣</sup>

$$\tau_s \propto \frac{T}{(\Delta G_m^v)^p D} \quad (1.1)$$

where

$\tau_s$  = time taken to establish a steady-state nucleation rate,

<sup>♣</sup> *The incubation time is in the actual analysis taken to be the time period before the onset of a detectable amount of isothermal transformation and this does not really coorespond to  $\tau_s$  as defined in Russell's equation.*

$T$  = absolute temperature,

$D$  = appropriate diffusion coefficient related to boundary or volume diffusion, depending on the coherency state of the nucleus concerned,

$p$  = an exponent, depending on the nature of the nucleus,

$\Delta G_m^v$  = the maximum volume free energy change accompanying the formation of a nucleus in a large amount of matrix phase.

Referring to equation 1.1, and using the theory of diffusion coefficients<sup>[50]</sup>, Bhadeshia obtained

$$D \propto \exp\left(\frac{S}{R}\right) \exp\left(\frac{-Q}{RT}\right) \quad (1.2)$$

where  $S$  is the activation entropy for diffusion and  $Q$  is the activation enthalpy for diffusion. Substituting this result in equation 1.1, assuming  $\tau = \tau_s$ , and multiplying  $\Delta G_m^v$  by the molar volume of ferrite, following relation was obtained

$$\ln \left[ (\Delta G_m)^p \frac{\tau}{T} \right] = \frac{Q}{RT} + C_1 \quad (1.3)$$

where  $\Delta G_m$  is the chemical free energy change accompanying the formation of 1 mol of nucleating system in a large amount of matrix phase and  $C_1$  is a constant.

#### 1.5.1.1 Calculation of Chemical Free Energy Change for Nucleation

Fig. 1.10 shows Gibbs free energy curves for austenite and ferrite as a function of their carbon concentrations. Let the carbon content of the alloy be  $\bar{x}$  and the free energy of  $\gamma$  of composition  $\bar{x}$  is represented by the point  $\bar{G}$ . The free energy of the specimen can be lowered as far as the point  $p$ , by the formation of a mixture of  $\gamma$  of composition  $x_\gamma^{\gamma\alpha}$  and  $\alpha$  phase of composition  $x_\alpha^{\alpha\gamma}$ . The precipitation process is initially very slow as the nucleation barrier must be overcome<sup>[51]</sup>. Because of the negligible volume of any nucleus, it may be assumed that its formation leaves the parent phase unchanged with respect to composition. Then, the formation of a nucleus with the composition  $x_m$  should involve transfer of the mole fraction  $x_m$  carbon atoms from a higher chemical potential state to a lower chemical potential state. From the geometry of the graph it can be seen that the free energy change is represented by the vertical distance  $\Delta G_m$  if the point  $m$  represents the free energy of the nucleus. Actually, the point  $m$  does not

represent the free energy of the nucleus (capillary effects are ignored as any dependence of surface energy on composition). From the diagram, it is apparent that the free energy change ( $\Delta G_m$ ) for nucleation will be maximum for a nucleus of composition  $x_m$  and ( $\Delta G_m$ ) can thus be calculated using the parallel tangent construction as illustrated.

The use of the nucleation composition corresponding to the maximum  $\Delta G_m$  is a very good approximation for steels, since the solubility of carbon in ferrite is so limited that any carbon concentration up to the equilibrium level makes small difference to the magnitude of  $\Delta G_m$ . Numerical value of  $\Delta G_m$  can be obtained from the following equation<sup>[52]</sup> deduced from Fig. 1.10

$$\Delta G_m = RT \ln \left| \frac{a_C^\alpha \{x_m\}}{a_C^\gamma \{\bar{x}\}} \right| \quad (1.4)$$

where  $a_C^\alpha \{x_m\}$  denotes the activity of carbon in the ferrite of composition  $x_m$  and  $a_C^\gamma \{\bar{x}\}$  denotes the activity of carbon in austenite of composition  $\bar{x}$ . The ideal nucleus composition,  $x_m$ , is determined by iterative solution of the equation<sup>[52]</sup>

$$\Delta G_{Fe}^{\gamma \rightarrow \alpha} + RT \ln \left\{ \frac{a_{Fe}^\alpha \{1-x\}}{a_{Fe}^\gamma \{1-\bar{x}\}} \right\} - RT \ln \left\{ \frac{a_C^\alpha \{x\}}{a_C^\gamma \{\bar{x}\}} \right\} = 0 \quad (1.5)$$

where  $\Delta G_{Fe}^{\gamma \rightarrow \alpha}$  is the free energy change accompanying the austenite to ferrite transformation in pure iron and  $R$  is the gas constant.  $a_{Fe}^\alpha \{1-x\}$  denotes the activity of iron in ferrite of composition  $(1-x)$  and other activity terms can be defined likewise. The values of  $p$  and  $D$  are fixed by a curve fitting to experimental data and  $\tau_s$  is assumed equal to  $\tau$  (the incubation time). Therefore, this method precludes any preconceived ideas regarding the shape, the coherency or the size of the initial nucleus. The method is capable of reproducing the critical bay region of the time-temperature-transformation (TTT) curves. The calculations generate two 'C' curves as function of time and temperature, one representing the reconstructive transformation and the other representing the displacive reactions (Widmanstätten ferrite, acicular ferrite and bainite) as illustrated in Fig. 1.11. It is also possible to predict relative shifts in these component curves, as a function of alloying element content. In the case of lower 'C' curve the diagram is truncated at the  $W_s$  (or  $B_s$ , when Widmanstätten ferrite formation is not possible), since this represents an upper limit for the Widmanstätten ferrite and bainite reactions.

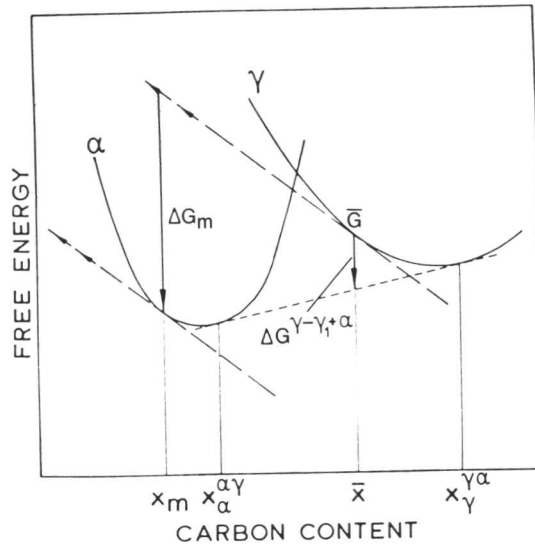


Fig. 1.10: Parallel tangent construction to find maximum free energy for the nucleation of ferrite.

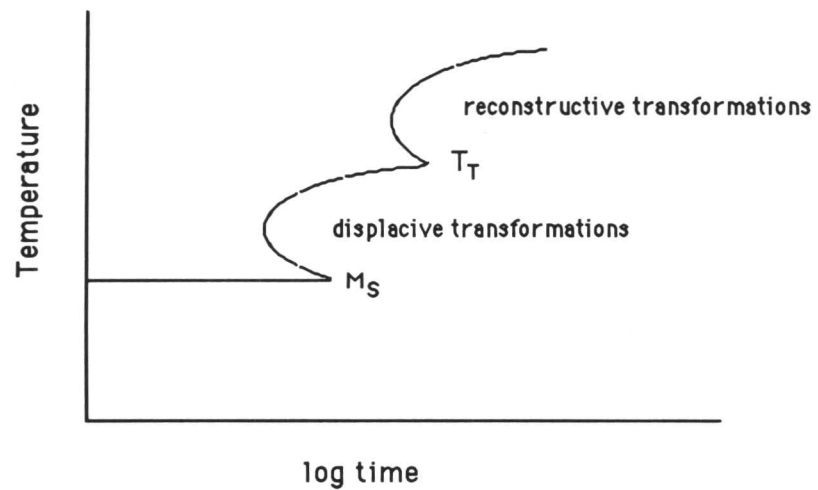
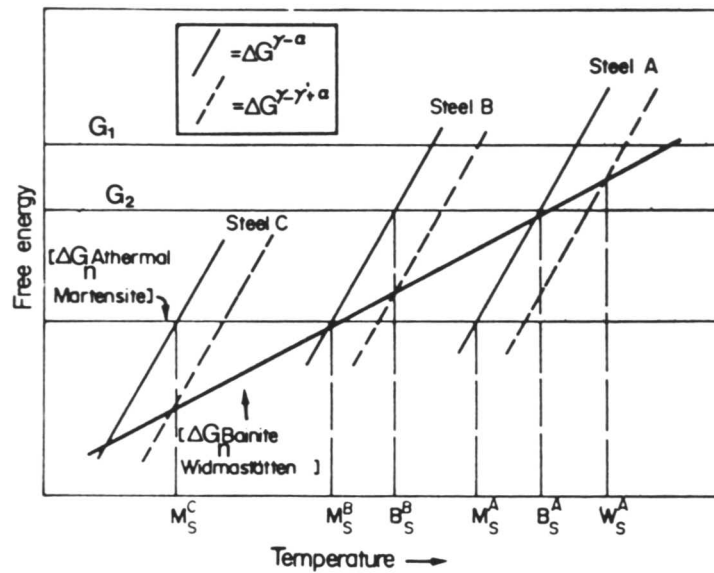


Fig. 1.11: A schematic time-temperature-transformation (TTT) diagram showing two distinct 'C' curves.

The analysis does not consider austenite grain size variations, but it has been pointed out<sup>[53]</sup> that such variations are relatively small at least as far as the onset of transformation is concerned. The calculations of Widmanstätten ferrite, bainite and martensite start temperatures are illustrated in Fig. 1.12. Both bainite and Widmanstätten ferrite nuclei are assumed to have the carbon concentration consistent with the maximum free energy change, although during growth the bainitic ferrite may become supersaturated with carbon. The temperature at which displacive products can be formed is decided by  $\Delta G_N$ , which is defined as the minimum free energy needed for the austenite to transform displacively to ferrite.



**Fig. 1.12:** Schematic representation of calculation of  $W_s$ ,  $B_s$ ,  $M_s$  temperatures for low (A), medium (B) and high alloy (C) compositions<sup>[22]</sup>. It should be noted that  $G_1=50 \text{ J/mol}$  and  $G_2=400 \text{ J/mol}$  are the stored energies of  $\alpha_W$  and  $\alpha_b$  respectively.  $\Delta G^{\gamma \rightarrow \alpha}$  is the free energy change accompanying the formation of  $\alpha$  of the same composition as  $\gamma$ . While  $\Delta G^{\gamma \rightarrow \gamma' + \alpha}$  is the free energy change accompanying the formation of ferrite which at all times contains an equilibrium carbon content. For alloy steels this term is computed on the basis of no substitutional element partitioning.

### 1.5.2 Phase Diagrams

The construction of the phase diagrams involves calculations of the phase boundary lines derived from the available free energy for transformation and is illustrated in Fig. 1.13. The calculations in the model are based on Lacher, Fowler and Guggenheim model<sup>[54]</sup>. Ferrite growth without a change in composition can only occur below the  $T_0$  temperature at which stress free  $\alpha$  and  $\gamma$  of identical composition have equal free energy<sup>[15]</sup>. The  $T_0$  temperature lies between the  $A_{e3}$  and  $A_{e1}$  temperatures which in turn define the upper and lower limits of the two phase  $\alpha + \gamma$  field. Bainite ( $\alpha_b$ ) and Widmanstätten ferrite ( $\alpha_W$ ), both grow by a displacive transformation mechanism. The formation of  $\alpha_W$  involves the redistribution of carbon between the parent and product phase, but  $\alpha_b$  initially forms by a diffusionless mechanism and the carbon later partitions into the remaining austenite. In the transformation of bainite, the whole of the austenite does not transform instantaneously. The transformation starts from the austenite grain boundaries; even though the initial plate forms without diffusion, it has an opportunity to reject its excess carbon into the residual austenite. Any further increment of transformation is, therefore, associated with a lower free energy change, due to the higher carbon content of the austenite from which it has to form. Eventually, a stage is reached when the transformation becomes thermodynamically impossible since the free energies of the residual austenite and bainite become identical<sup>[15,22,52,55]</sup>. The locus of such positions, as a function of isothermal transformation temperature defines the  $T'_0$  curve<sup>\*</sup> (Fig. 1.13), where  $\gamma$  and  $\alpha_b$  (with a certain amount of stored energy associated with transformation strains) of the same composition have equal free energies.

The bainite reaction should therefore stop when the carbon concentration of the austenite reaches the level given by the  $T'_0$  for the isothermal transformation temperature concerned. The  $A'_{e3}$  curve may be similarly defined for the growth of  $\alpha_W$ , which involves the paraequilibrium transformation with the partitioning of carbon, (but not of substitutional alloying elements). For plain carbon steels, it follows that the  $A'_{e3}$  and

---

<sup>\*</sup> *The  $T'_0$  curve is the  $T_0$  curve modified to take account of the strain energy accompanying the Invariant Plane Strain (IPS) shape change during transformation. Invariant Plane Strain may be regarded as a simple shear on the invariant-plane, together with an expansion or contraction normal to this plane<sup>[57]</sup>.*

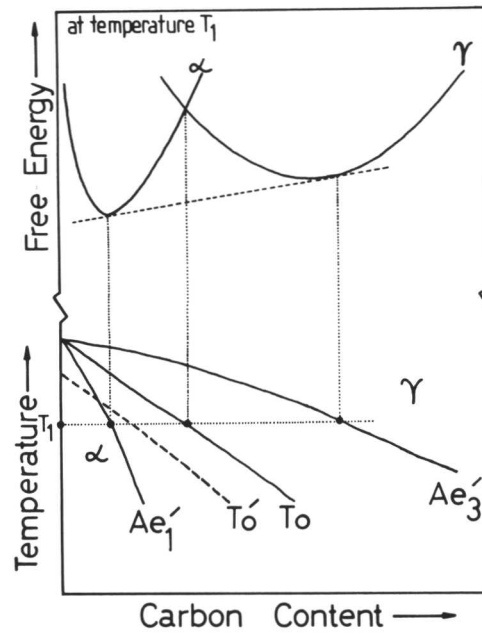


**Fig. 1.13:** Schematic diagram showing the construction of phase boundaries from free energy data. The  $T_0$  line includes the effect of 400 J/mol of strain energy due to transformation (after Yang and Bhadeshia<sup>[56]</sup>).

$A_{e3}$  curves are identical. The aim of this project is to predict development of microstructure in chemically heterogeneous alloys using the above model as a basis.

## REFERENCES

1. G. J. Davies: *Solidification and Castings*, Applied Science Publishers, London, 1973.
2. M. C. Flemings: *Solidification Processing*, McGraw-Hill, New York.
3. G. J. Davies and J. G. Garland: *Int. Met. Rev.*, 1975, vol. 20, p. 83.
4. W. F. Savage: *Welding in the World*, 1980, vol. 18, p. 89.
5. W. F. Savage *et al.*: *Welding J.*, 1965, vol. 44, p. 175.
6. W. F. Savage and A. H. Aronson: *Welding J.*, 1966, vol. 45, p. 85.
7. R. A. Woods and D. R. Milner: *Welding J.*, 1971, vol. 50, p. 164s.
8. H. K. D. H. Bhadeshia: *Phase Transformations 87'*, p. 309, ed. G. W. Lorimer, Institute of Metals, London, 1988.
9. C. S. Smith: *Trans. A. S. M.*, 1953, vol. 45, p. 533.
10. R. W. K. Honeycombe: *Perspectives in Metallurgical Development*, p. 163, The Metal Society, London, 1984.
11. M. Hillert: *The Decomposition of Austenite By Diffusional Process*, p. 197, Interscience, New York, 1962.
12. E. Levine and D. C. Hill: *Met. Constr.*, 1977, vol. 8, p. 346.
13. J. H. Tweed: *Ph.D. Thesis*, University of Cambridge, 1982.
14. J. W. Cahn and J. E. Hilliard: *J. Chem. Phys.*, 1958, vol. 29, p. 258.
15. H. K. D. H. Bhadeshia: *Prog. in Mat. Sci.*, 1985, vol. 29, p. 321.
16. J. H. Develtian and W. E. Wood: *Metals Handbook*, p. 21, A. S. M., Metals Park, Ohio, 1983.
17. L. G. Taylor, R. A. Farrar, *Weld. Met.*, 1975, vol. 43, p. 305.
18. H. K. D. H. Bhadeshia and D. V. Edmonds: *Metall. Trans.*, 1979, vol. 10A, p. 895.
19. J. W. Christian and D. V. Edmonds: *Phase Transformations in Ferrous Alloys*, p. 293, editors A. R. Marder and J. I. Goldstein, The Metallurgical Society of AIME, Warrendale, 1983.
20. H. K. D. H. Bhadeshia and J. W. Christian: *Bainite in Steels*, Conf. Proc., A. S. M. International, Chicago, September, 1988.

21. H. I. Aaronson, C. Laird and K. R. Kinsman: *Phase Transformations*, 1970, A. S. M., p. 313.
22. H. K. D. H. Bhadeshia: *Acta Metall.*, 1981, vol. 29, p. 1117.
23. H. K. D. H. Bhadeshia: *J. of Mat. Sci.*, 1983, vol. 18, p. 1473.
24. M. Takahashi and H. K. D. H. Bhadeshia: *Mat. Sci. and Tech.*, 1990, in press.
25. H. K. D. H. Bhadeshia: *Acta Metall.*, 1980, vol. 28, p. 1103.
26. G. R. Srinivasan and C. M. Wayman: *Acta Metall.*, 1968, vol. 16, p. 609.
27. M. Strangwood and H. K. D. H. Bhadeshia: *Advances in Welding Science and Technology*, p. 209, editor S. A. David, A. S. M. Metal Park, Ohio, 1987.
28. J. R. Yang and H. K. D. H. Bhadeshia: *Advances in Welding Science and Technology*, p. 187, editor S. A. David, A. S. M. Metal Park, Ohio, 1987.
29. R. A. Ricks, G. S. Barritte and P. R. Howell: *Solid → Solid Phase Transformations*, p. 463, editors H. I. Aaronson *et al.*, Metallurgical Society of AIME, 1981.
30. S. Liu and D. L. Olson: *Weld. J. Res. Suppl.*, 1986, p. 139s.
31. D. J. Widgery: *Ph.D. Thesis*, University of Cambridge, U. K., 1974.
32. J. G. Garland and P. R. Kirkwood: *Met. Constr.*, 1975, vol. 7, p. 275.
33. R. A. Roberts and R. F. Mehl: *Trans. A. S. M.*, 1943, vol. 31, p. 613.
34. C. L. Magee: *Phase Transformations*, p. 115, ASM, Metals Park, Ohio, 1959.
35. G. B. Olson and M. Cohen: *Ann. Rev. Mater. Sci.*, 1981, p. 1.
36. J. S. Kirkaldy: *Can. J. Phys.*, 1958, vol. 36, p. 907.
37. M. Hillert: *Met. Trans.*, 1975, vol. 6A, p. 5.
38. G. R. Purdy, D. H. Weichert and J. S. Kirkaldy: *TMS-AIME*, 1964, vol. 230, p. 1025.
39. M. Hillert: *The Mechanism of Phase Transformation in Crystalline Solids*, p. 231, Monograph No. 13, Institute of metals, London, 1969.
40. D. E. Coates: *Metall. Trans.*, 1973, vol. 4, p. 2313.
41. J. S. Kirkaldy: *Adv. Mater. Res.*, 1970, vol. 4, p. 55.
42. A. Hultgren: *Jernkontorets Ann.*, 1951, vol. 135, p. 403.
43. H. K. D. H. Bhadeshia, L. E. Svensson and B. Gretoft: *Acta. Metall.*, 1985, vol. 33, p. 1271.
44. H. K. D. H. Bhadeshia, L. E. Svensson and B. Gretoft: *J. of Mater.*, 1985, vol. 4, p. 305.

45. L. E. Svensson, B. Greftoft and H. K. D. H. Bhadeshia: *Scand. J. of Metallurgy*, 1986, vol. 15, p. 97.
46. B. Greftoft, H. K. D. H. Bhadeshia and L. E. Svensson: *Acta Stereologica*, 1986, p. 365.
47. H. K. D. H. Bhadeshia, L. E. Svensson and B. Greftoft: *Advances in Welding Science and Technology*, p. 225, editor S. A. David, A. S. M. Metal Park, Ohio, 1987.
48. H. K. D. H. Bhadeshia, L. E. Svensson and B. Greftoft: *Welding and Performance of Pipelines*, p. 17-1, editor P. H. M. Hart, The Welding Institute, Abington, 1986.
49. K. C. Russell: *Acta Metall.*, 1969, vol. 17, p. 1123.
50. J. W. Christian: *Theory of Transformations in Metals and Alloys*, p. 375, Pergamon, Oxford, Pt. 1, 2nd ed., 1975.
51. M. Hillert: *Acta Met.*, 1953, vol. 1, p. 764.
52. H. K. D. H. Bhadeshia: *Metal Science*, 1982, vol. 16, p. 159.
53. BISRA, *Special Report no. 56*, Chapman and Hall Ltd., London, 1956.
54. G. J. Shiflet, J. R. Bradley and H. I. A. Aaronson: *Metall. Trans.*, 1978, vol. 9A, p. 999.
55. H. K. D. H. Bhadeshia: *Journal de Physique*, vol. C4, p. 443.
56. J. R. Yang and H. K. D. H. Bhadeshia: *Trends in Welding Research*, p. 187, Tennessee, 1986.
57. H. K. D. H. Bhadeshia: *Scripta Met.*, 1987, vol. 21, p. 1017.

## Chapter 2

# HETEROGENEITY AND PHASE TRANSFORMATIONS

### 2.1 Introduction

Most industrial alloys usually have some degree of chemical heterogeneity, because they undergo thermo-mechanical treatments which are generally inconsistent with the achievement of thermodynamic equilibrium. Chemical segregation can have a profound influence on allotropic transformations and consequently on microstructure and properties, especially when the general level of alloying additions is large. This work is an attempt to understand quantitatively the manner in which composition fluctuations, of the kind encountered in industrial practice, influence both the nucleation and growth characteristics of solid-state phase transformations, and ultimately to relate the work to the influence of segregation on mechanical properties.

### 2.2 Chemical Heterogeneity

Segregation, which results in compositional heterogeneity in cast steels, is primarily an effect of non-equilibrium primary crystallization from the melt. The degree of heterogeneity depends on the amount and nature of the alloying elements and impurities present, and the cooling conditions. In general, the wider the crystallization temperature range, or more precisely, the greater the range of equilibrium concentrations represented during crystallization between the liquid and solid phases, the greater the segregation. Segregation is generally classified as:

- (a) microsegregation, which extends over distances of the grain diameter or less and
- (b) macrosegregation, which can extend over many grain diameters.

#### 2.2.1 Solute Redistribution

Consider the solidification of an alloy of mean composition  $X_0$  in the binary system as shown in Fig. 2.1. According to solidification theory, any of the following three limiting cases may govern the transformation<sup>[1]</sup>:

- Solidification occurs under complete equilibrium conditions.
- Solidification is not an equilibrium process and no diffusion occurs in the solid, but perfect mixing occurs in the liquid.

- Solidification is not an equilibrium process, no diffusion occurs in the solid, and the mixing in the liquid is not perfect but occurs by diffusional processes only.

In practice, solidification does not occur under equilibrium conditions, so the first point can be neglected. To begin with, the assumption that the negligible diffusion in the solid phase is a good first approximation to make. In the initial stages of solidification good mixing of the liquid seems likely due to turbulence in the melt.

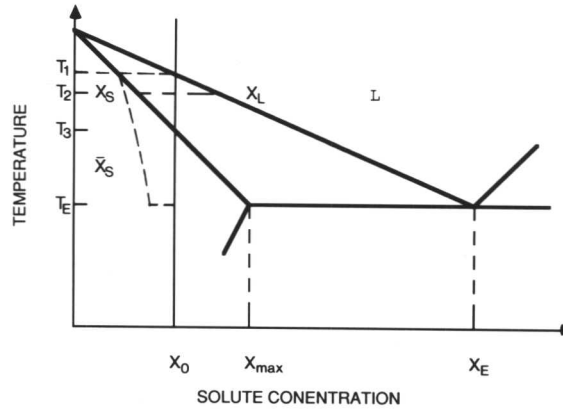


Fig. 2.1: The non-equilibrium solidification of an alloy,  $X_0$ , in a binary system<sup>[1]</sup>.

Consider the unidirectional solidification of a volume element of an alloy of composition  $X_0$  (Fig. 2.1) which has a liquidus temperature  $T_1$ . The first solid to form contains  $kX_0$  of solute and it will be purer than the liquid from which it forms, as  $kX_0 < X_0$ , where  $k$  is the partition coefficient<sup>♣</sup>. Due to the solute enrichment of the liquid, its new liquidus temperature will be lower than  $T_1$ . As this sequence of events continues the liquid becomes progressively richer in solute and solidification occurs at progressively lower temperatures. Since, initially, there is perfect mixing of the melt, for a given temperature the compositions of the solid and liquid in contact with one another are given by the equilibrium phase diagram (Fig. 2.1). However, as there is no diffusion in the solid the separate layers of solid retain their original composition so that

<sup>♣</sup> The partition coefficient ( $k$ ) of an element is the ratio of the equilibrium concentration of the element in the solid to its equilibrium concentration in the liquid phase, i.e.,  $k = \frac{X_s}{X_L}$ .

the mean composition of the solid is continuously lower than the solidus composition given by the phase diagram. The true solidus is defined by  $X_s$  in Fig. 2.1. On the other hand, the liquid becomes progressively richer in solute and may even attain eutectic composition at the temperature  $T_E$ . The corresponding composition profile will thus progress as shown in Fig. 2.2. The completely solidified volume element will then have a solute distribution as shown in Fig. 2.2c with  $\bar{X}_s = X_0$ . The variation of  $X_s$  along the solidified volume element can be obtained<sup>[2]</sup> by equating the solute rejected into the liquid when a small amount of solid forms with the resulting increase of solute in the liquid. Ignoring the difference in molar volumes between the solid and liquid this gives:

$$(X_L - X_s)df_s = (1 - f_s)dX_L \quad (2.1)$$

where,  $f_s$  is the volume fraction solidified.

Integrating this equation using the boundary condition  $X_s = kX_0$  at  $f_s = 0$  gives<sup>[2]</sup>

$$X_s = kX_0(1 - f_s)^{(k-1)} \quad (2.2)$$

and

$$X_L = X_0 f_L^{(k-1)} \quad (2.3)$$

$X_s$  and  $X_L$  are the mole fraction of solute in the solid and liquid in equilibrium at a given temperature.

Equations 2.2 and 2.3 are known as the non-equilibrium lever rule or the Scheil's equations. It should be noted that for  $k < 1$ , these equations predict that when there is no diffusion in the solid there will always be some eutectic in the last drop liquid to solidify, no matter how little solute is present. However, as the solidification goes to completion it seems likely that convectional mixing gives way to diffusional mixing. Thus, there will be a build-up of solute ahead of the growing crystal, with a correspondingly rapid increase in alloying content of the solid that forms as shown in Fig. 2.3a. If solidification is made to occur at a constant rate,  $v$ , it can be shown that a steady state is finally obtained when the interface temperature reaches  $T_3$  in Fig. 2.1.

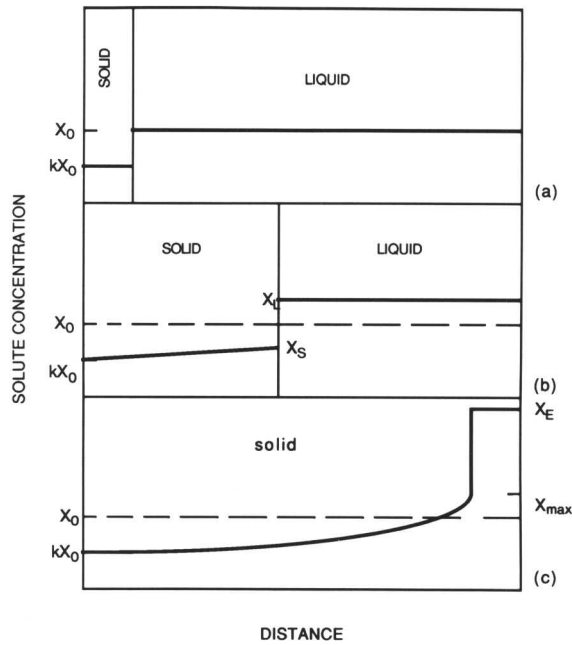


Fig. 2.2: The composition profile in a solidifying cylindrical bar under conditions of perfect mixing in the liquid and no diffusion in the solid<sup>[1]</sup>.

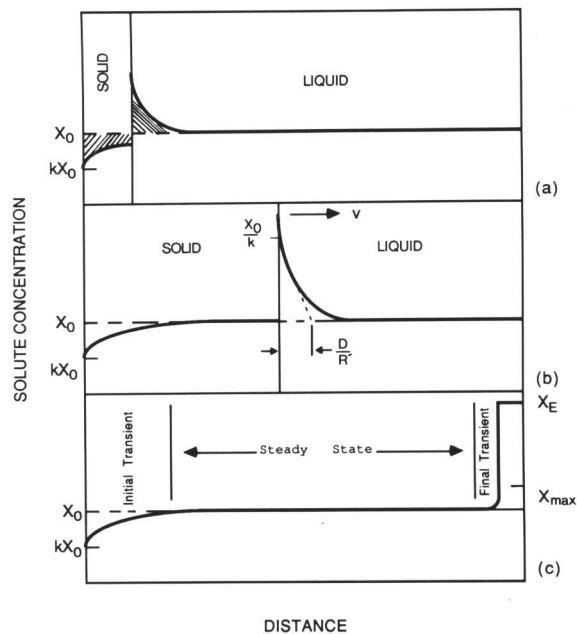


Fig. 2.3: The composition profile of a solidifying bar under conditions of no diffusion in solid but with diffusional mixing in liquid<sup>[1]</sup>.

During steady-state growth the concentration profile in the liquid must be such that the rate at which solute diffuses down the concentration gradient away from the interface is balanced by the rate at which solute is rejected from the solidifying liquid, *i.e.*,

$$\frac{-dX_L}{dx}D = R'(X_L - X_s) \quad (2.4)$$

where  $D$  is the diffusivity of the solute in the melt,

$\frac{dX_L}{dx}$  refers to the concentration gradient into the liquid and

$R'$  is the growth speed of the crystal. If the diffusion equation is solved for steady-state solidification it can be shown that the concentration profile in the liquid ahead of the interface is given by the following equation

$$X_L = X_0 \left[ 1 - \frac{1-k}{k} \exp\left(\frac{-xR'}{D}\right) \right] \quad (2.5)$$

This equation indicates that  $X_L$  decreases exponentially from  $\frac{X_0}{k}$  at  $x = 0$  (*i.e.*, the interface) to  $X_0$  at some large distance from the interface.  $\frac{D}{R'}$  gives the characteristic width of the concentration profile. In the final stages of solidification, the 'bow-wave' of solute is compressed into a comparatively small volume of liquid and the solute concentration is thus expected to rise rapidly as in Fig. 2.3c. In terms of weld solidification, this suggests that the last stages of weld solidification are associated with the highest level of segregation. Miller<sup>[3]</sup> has established the presence of a solute-rich layer ahead of the advancing solid/liquid interface in a weld pool and, using microprobe analysis on back-filled weld metal cracks, has also shown that the values of the equilibrium distribution coefficients for a variety of solute elements are the same in both weld-pool solidification and ingot solidification. The basic mechanism of solute segregation thus appears to be the same in both cases and, just as in ingot solidification, microsegregation is more pronounced in a weld bead, the more dendritic is the solidification mode.

### 2.2.2 Segregation

Segregation is classified as either microsegregation (extending over distances of the grain diameter or less) or macrosegregation (extending over more than several grain diameters). In turn microsegregation is subdivided into cellular, dendritic and grain boundary segregation. In the welds, at the side of the pool steep thermal gradients together with comparatively low solidification rates favour cellular growth while at the weld centre line, high solidification rates promote a transition to dendritic growth modes. The detailed nature of the segregation pattern is dependent on the growth conditions and morphology of the growing dendrites and is largely a manifestation of liquid flow in the semi-solid region<sup>[4-8]</sup>.

The segregation behaviour of a steel depends largely on whether ferrite or austenite forms during non-equilibrium solidification. An alloy has the lowest free energy when it is in a homogeneous condition, and this is the driving force for diffusion. There is a large difference in the rate of diffusion of alloying elements in these two phases. Because  $\gamma$ -iron has a close-packed crystal structure whereas  $\alpha$ -iron is more loosely-packed. The latter allows easier passage through the structure of vacancies and associated solute atoms. As a general rule, it may be stated that the diffusion coefficient doubles for every 20 °C rise in temperature. Table 2.1 shows typical diffusion coefficients of different alloying elements in  $\alpha$  and  $\gamma$  at 700 °C.

$D_\alpha$  and  $D_\gamma$  are the diffusion coefficients in  $\alpha$  and  $\gamma$  respectively. In contrast to carbon, the diffusion rate in austenite for substitutionally dissolved elements is very low and only a small amount of alloying elements can pass through austenite from the liquid into the ferrite.

Numerical calculations for austenite show that so-called back diffusion<sup>♣</sup> is important only towards the end of the solidification, and hardly effects the central parts of the dendrite arms. Calculations for ferrite indicate that back diffusion is very significant, and a dendrite arm can have an almost uniform composition just behind the solidification front.

---

♣ *Back diffusion is the diffusion of alloying elements from the liquid to the solid due to concentration gradient established between the two during solidification.*

ALLOYING ELEMENT	$D_{\alpha}$ cm <sup>2</sup> /s	$D_{\gamma}$ cm <sup>2</sup> /s
Mo	$6.11 \times 10^{-12}$	$8.72 \times 10^{-14}$
Ni	$5.09 \times 10^{-12}$	$1.73 \times 10^{-14}$
Cr	$4.79 \times 10^{-11}$	$1.51 \times 10^{-14}$
Si	$1.30 \times 10^{-7}$	$4.00 \times 10^{-10}$
C	$2.36 \times 10^{-6}$	$1.77 \times 10^{-8}$

**Table. 2.1:** Diffusion coefficients<sup>[9-11]</sup> of different alloying elements in  $\alpha$  and  $\gamma$ . However it should be noted that the data represent a simplification as these coefficients are concentration dependent.

Using an approximate method Brody and Flemings<sup>[12]</sup>, derived an equation to take account of back diffusion.

$$X_l = X_0 \left[ \frac{1-f}{1+A} \right]^{-(1-k)} \quad (2.6)$$

Where A is a parameter defined as follows:

$$A = \frac{kD^s\theta}{\lambda^2}$$

where

$D^s$ =diffusion constant in solid state,

$\theta$  =the total solidification time,

$\lambda$ =half of the dendrite arm spacing, and

$X_0$ =composition of the alloy.

The “A” term depends on the back diffusion and is a correction term to the original Scheils’ equations.

The equation shows that, as long as the 'A' term is much less than  $(1 - f)$ , the distribution can be fairly well described by the original Scheil's segregation equation. As  $(1 - f)$  grows smaller towards the end of the solidification process, the importance of back diffusion increases. This is an effect of the very steep concentration gradient at the end of the solidification process. Segregation is also influenced by differences in the partition coefficients between ferrite and liquid, or austenite and liquid, for different alloying elements; the cooling rate will also have a major effect. The nature of the liquid  $\rightarrow$  solid transformation can itself have an important effect; in steels, primary solidification phase may be  $\delta$ -ferrite or austenite. The intensity of segregation is expressed in a convenient, quantitative manner by the segregation ratio " $S_i$ " for an alloying element " $i$ ". It is defined as the ratio between the highest and lowest values of the concentration in a dendrite. This quantity can be calculated by applying equation 2.6 at  $f = 0$  and  $f = 1$ , assuming that  $X_s = kX_l$  in both cases.

$$S = \left( \frac{1 + A}{A} \right)^{1-k} \quad (2.7)$$

The segregation ratio increases with increasing cooling rate and with decreasing partition coefficient<sup>[13]</sup>. Table 2.2 shows the calculated partition coefficients between  $\delta$ -iron and liquid ( $k_i^{\delta/l}$ ) and between austenite and liquid ( $k_i^{\gamma/l}$ ). Flemings<sup>[14]</sup> has tabulated experimental results for microsegregation in some iron based alloys; these values are shown in Table 2.3, where  $S_i$  varies from 1.0 to over 4.0.

Among the metals, Mn should produce extensive segregation on a dendritic scale<sup>[16]</sup>. This is due to the fact that the addition of Mn to Fe-C alloys extends the  $\gamma$  phase region in the Fe-C diagram as shown in the Fig. 2.4.

Alloys with higher C and Mn contents can solidify directly to austenite<sup>[17]</sup>. If that happens, the heterogeneity of the  $\gamma$ -solution is considerably higher than for the case of primary  $\delta$  solidification, since there is a greater range of equilibrium concentrations represented during the direct solidification of the melt to  $\gamma$ -solution, and because the solid state diffusion of substitutional elements is more sluggish in austenite so that homogenisation during cooling is also more sluggish. Cu, Sn, Mo, W, V, and probably Co also exhibit appreciable segregation. Nickel produces a fairly small dendritic segregation, Cr and Si generally produce only slight dendritic segregation.

ALLOYING ELEMENT wt. %	$\frac{\delta}{k}$	$\frac{\gamma}{k}$
C	0.06	0.29
Mn	0.76	0.81
Si	0.69	0.65
Ni	0.45	0.58
Cr	0.81	0.81
Mo	0.48	0.38
V	0.74	0.72

Table. 2.2: Partition coefficients calculated, to a first approximation, by the expression<sup>[15]</sup>  $k_i = e^{\frac{\Delta G_i^0}{RT}}$ , of alloying element 'i'.  $\Delta G_i^0$  is the Gibbs free energy change per mole in transferring the pure element 'i' from the  $\delta$  to the liquid state and 'R' is the universal gas constant.

Alloy	Alloying Element	Distance From The Chill (mm)	Segregation Ratio
Fe-10Ni	Ni	12.5	1.35
		50.0	1.38
Fe-26Ni	Ni	12.5	1.28
		50.0	1.17
Fe-26Ni-33C	Ni	50.0	1.19
Fe-0.4C-1.8Ni-0.8Cr-0.7Mn	Mn	43.0	1.5
		145.0	1.8
	Ni	43.0	1.2
		145.0	1.5
Fe-1.5Cr	Cr	12.5	1.0
Fe-1.5Cr-1.0C	Cr	12.5	4.0
		50.0	4.1

Table. 2.3: Experimental values of the segregation ratios (after Flemings<sup>[14]</sup>).

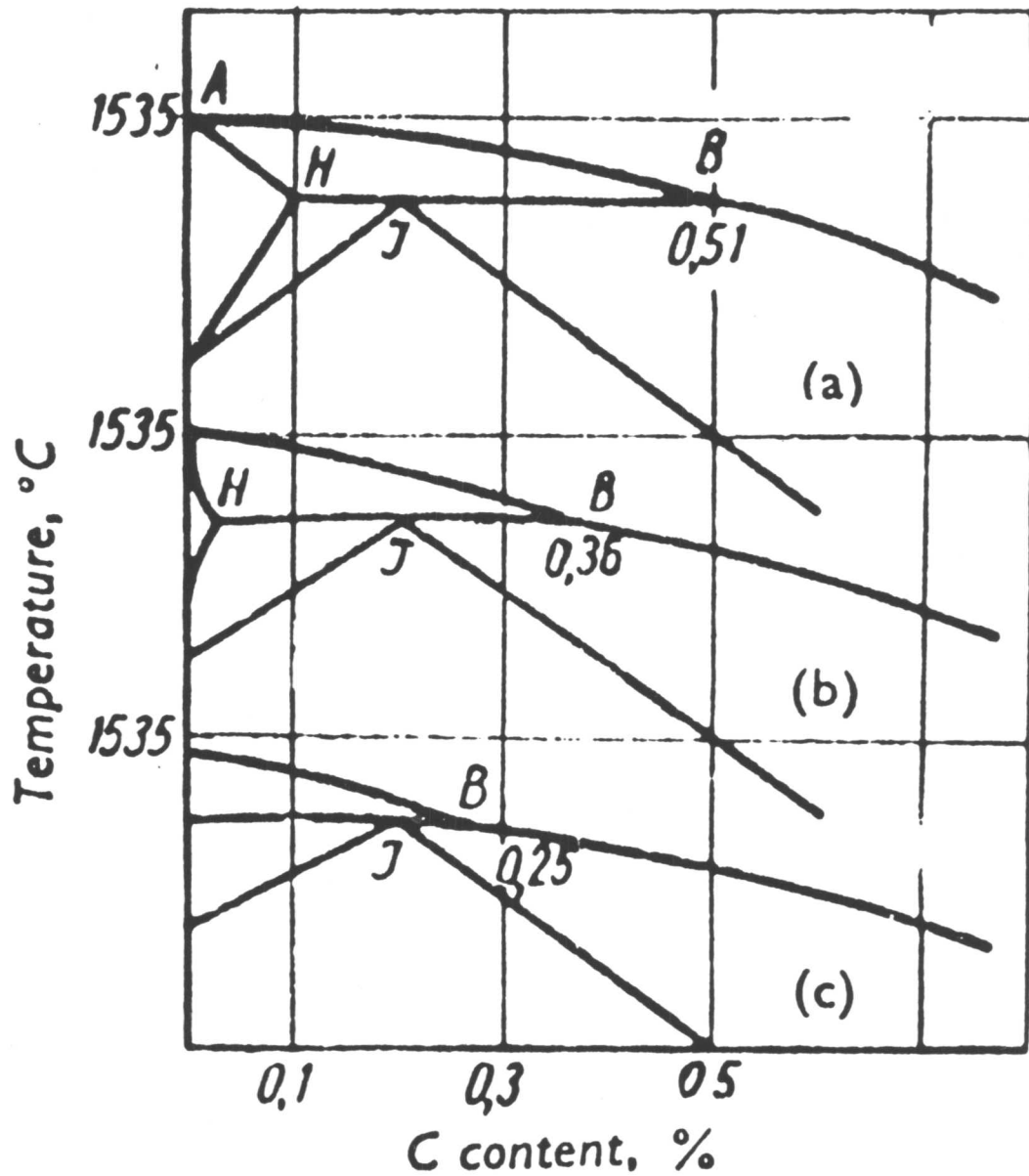


Fig. 2.4: The addition of Mn to Fe-C alloys extends the  $\gamma$ -phase region in the diagrams for,

- (a) a steel without Mn,
- (b) a steel with 1.5 wt. % Mn,
- (c) a steel with 2.5 wt. % Mn.

Among the non-metals, C, P, and S can be considered to have a marked ability to produce segregation, but the diffusion of one can be greatly affected by the presence of the others, as well as by other metal constituents. During solidification, the inclusions themselves are also subject to large and small scale spatial segregation. The silicate inclusions are concentrated in the arms of the dendrites, while the sulphur inclusions are usually located in the interdendritic spaces<sup>[18]</sup>. An interesting observation has been the discovery of inclusion segregation<sup>[19]</sup> in steel weld deposits, when the inclusions found at the cellular solidification boundaries.

Although the intensity of microsegregation is determined by the composition, the periodicity is controlled by the dendrite arm spacing. The dendrite arm spacing varies inversely with cooling rate to a power of between one-third and one-half<sup>[20]</sup>.

### *2.2.3 Banding*

For castings it has been proposed<sup>[21]</sup> that solute-rich or solute-poor areas can result from fluctuations in the position of the growing liquid/solid interface. These fluctuations can be the result of periodic changes in heat flow and are analogous to those observed in arc welds when the arc energy is varying. Solute banding, which is a periodic enrichment and depletion of solute elements, is frequently observed in both manual and automatic welding, made with or without filler additions. When steel ingots are deformed the segregated areas are elongated into bands; a macroscopically laminated structure can therefore be caused by dendritic segregation. The banded structure proper which is found in worked materials under certain conditions has been investigated especially for annealed hypoeutectoid carbon steels. The reason seems to be that the alloys with this range of carbon content undergo direct melt to  $\gamma$ -solution transformation and experience a greater range of equilibrium concentrations during solidification, thus, resulting in greater segregation. Banding is favoured by austenitizing slightly above the  $A_{c3}$  point or, better still, between  $A_{c3}$  and  $A_{c1}$  temperatures. This is because the  $A_{c3}$  temperature is raised relative to the  $A_{c1}$  temperature under the influence of most segregated alloy elements (Fig. 2.5).

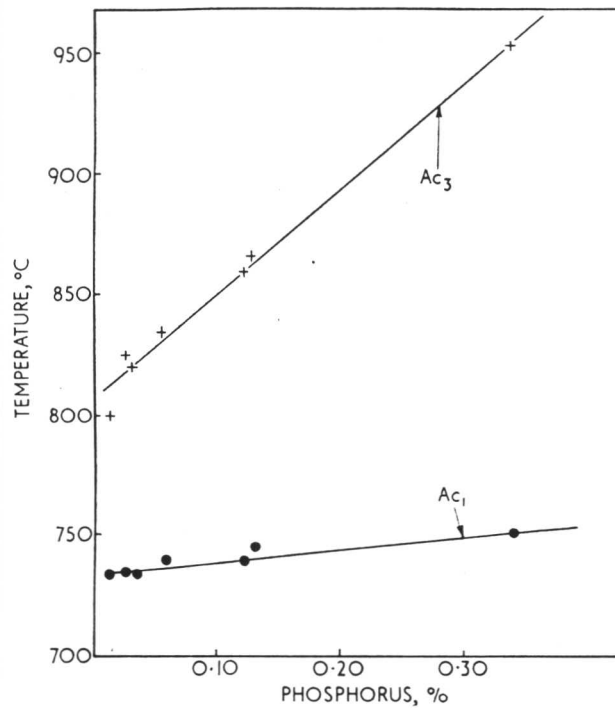
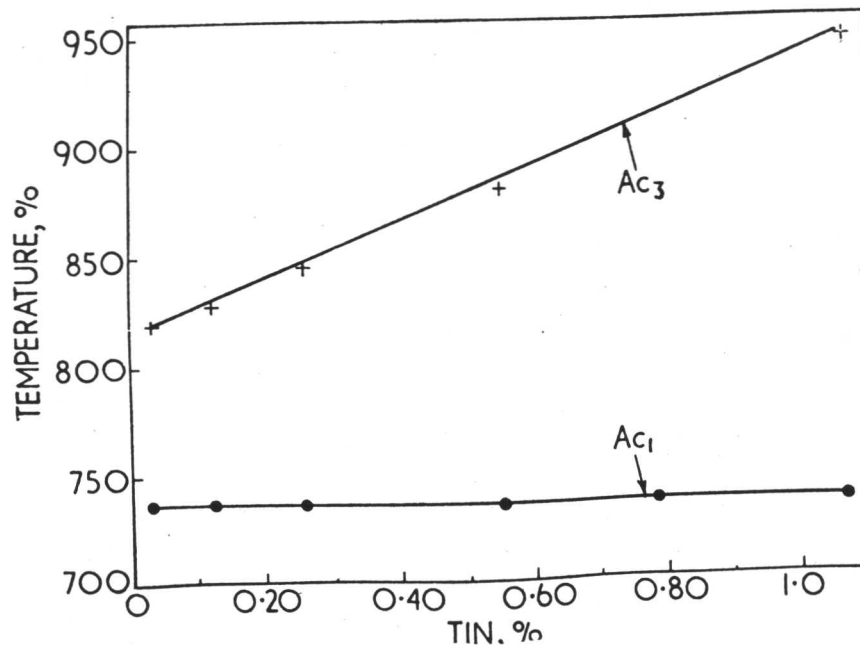


Fig. 2.5: Influence of alloying elements on the position of  $Ac_1$  and  $Ac_3$  temperatures (after Bastein, 1957).

(a) Influence of phosphorus.

(b) Influence of tin.

There has been general agreement for a number of years that the appearance of alternate pearlite and ferrite bands in rolled and forged hypoeutectoid steel products is primarily associated with persistent segregation of alloying elements other than carbon. This segregation originates in normal interdendritic segregation during solidification of the ingot, and because of the slow diffusion of many elements, particularly substitutional ones, at working and soaking temperatures, it persists in a more or less moderated form into the final product in a laminar distribution.

Jatczak *et al.* [22] regard the banding as being due to the opposing effects of solution elements and carbide formers on the location of carbon through their effect on the carbon activity in austenite at soaking temperatures, during cooling and during transformation. They found that carbide forming elements tend to increase carbon concentration in their vicinity, while solution type elements (e.g. Ni, Si, etc) tend to decrease carbon concentration in their vicinity. Therefore, in Fe-C-X type steels, the degree of carbon segregation and the location of high and low carbon areas relative to a fixed marker depends solely on the amount and distribution of the one alloying element, *i.e.*, X. In multi-alloyed steels, these bands depend upon a balanced influence as determined by alloy types, amounts and distribution [22].

Bastien [18], on the other hand, emphasizes the role of the constitutional effect of the alloying elements in shifting the  $Ar_3$  line, resulting in premature or delayed nucleation of proeutectoid ferrite. He suggests for example, in the case of P segregation, that since P-rich regions have a higher  $Ar_3$  temperature the proeutectoid reaction will begin in these regions, rejecting carbon to P-depleted regions, and delaying the beginning of transformation there even further. However, in the case of P banding, the Jatczak [22] and Bastien [18] views are both tenable, since it is known that P increases the activity<sup>♣</sup> of carbon in austenite and will accordingly tend to repel carbon.

Kirkaldy *et al.* [23] examined quantitatively the banding behaviour in the ternary systems Fe-Si-C, Fe-Mn-C, Fe-Ni-C, Fe-Cr-C and Fe-P-C both as to the intensity of carbon segregation which occurs in the soaking (austenite) range and during the subsequent  $\gamma$  to  $\alpha$  transformation. The results confirm that the segregation of carbon which occurs before transformation is due to the equalization of the carbon activities. As

---

<sup>♣</sup> *Activity is a thermodynamic function representing the change in the behaviour of a dissolved substance relative to the pure one.*

expected from thermodynamic data, Si, Ni and P rich regions reject carbon, while Mn and Cr rich absorb it. They showed that the magnitude of carbon pre-segregation<sup>♣</sup> is in all cases only a fraction of the mean concentration, and does not increase significantly as the temperature is lowered towards the transformation temperature. Accordingly, the intense segregation which occurs in the room temperature microstructure of banded steels cannot be attributed to this phenomenon alone. However, this pre-segregation significantly influences the difference in  $A_{e_3}$  temperature between adjacent layers and with it the sequence of ferrite nucleation across a segregated steel. Hence, pre-segregation affects the nucleation sequence by increasing the difference in nucleation temperature.

In evaluating the degree to which certain elements are responsible for banding, one must determine the extent to which each element is segregated during the initial solidification of the melt, and the rate at which the segregation will be reduced by diffusion. Qualitatively, we may assume that large partition coefficients and low diffusion coefficients will favour banding<sup>[23]</sup>. Jaczak *et al.* <sup>[22]</sup> found that isothermal treatment is more sensitive to the development of banded structures than is the case during continuous cooling but they did not go into any details of the transformations. Isothermal transformation results obtained by them are shown in the figure 2.6 for the Fe-0.42C-0.72Mn-0.29Si-0.82Cr-1.74Ni-0.25Mo wt. % steel.

Inclusions in steel which have been arranged into laminar through plastic deformation can, at least theoretically, play a part in the formation of the banded structure, either by favouring the physico-chemical reaction at the interfaces, or by locally modifying the chemical composition of the steel and thus altering its transformation points if they are slightly soluble in iron at a high temperature. According to Bastien<sup>[18]</sup>, any theories which ascribe to the inclusions an essential role in the formation of banded structure are, however incorrect; for a given steel and for different cooling rates, inclusions of a particular type may sometimes be found in the ferrite and some times in the pearlite. Other reasons for rejecting such theories is the effect of a homogenization treatment at a high temperature which partly destroys the banded structure without affecting the inclusions.

---

<sup>♣</sup> *Carbon pre-segregation refers to the segregation of carbon which occurs in the soaking range or before transformation.*

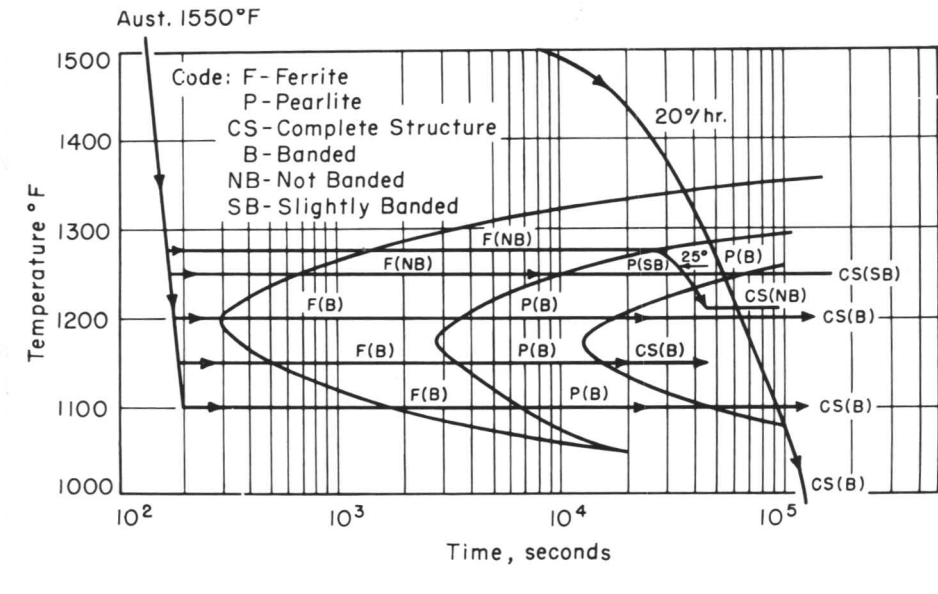


**Fig. 2.6:** Effect of isothermal and continuous cooling on banding in Fe-0.42C-0.72Mn-0.29Si-0.82Cr-1.74Ni-0.25Mo wt. % (after Jatzcak et al. [22]).

### 2.3 Homogenization

It has been found out<sup>[18]</sup> that the banded microstructure disappears when the cooling rate exceeds a certain value, which varies from one steel to another. Although the microstructural banding vanishes, but compositional banding does not. Hence, this disappearance of the banded microstructure is only temporary, and a further heat-treatment followed by slower cooling causes it to reappear. Small scale segregation can be removed by means of a long heat treatment at a high temperature in the austenite phase field, thus making the material chemically homogeneous. This is rarely the case in practice, mainly because of the low diffusion rates of most of the dissolved elements (except carbon) and also because of very low solubility of non-metallic inclusions in the solid state in iron. This segregation therefore persists, although to a more or less reduced extent, even after the high temperature heat treatments used for large forgings. Hence, the effectiveness of a homogenization treatment diminishes with increasing size of the forging, and especially near its centre<sup>[18]</sup>.

Several investigations on this subject have shown that complete homogenization is very difficult to achieve and that in some cases it is necessary to raise the temper-

ature to 1300 which introduces other difficulties, such as overheating\* of the steel<sup>[24]</sup>. Certain workers<sup>[25]</sup> have noted a relationship between the width of the bands and the temperature necessary to suppress them as shown in figure 2.7.

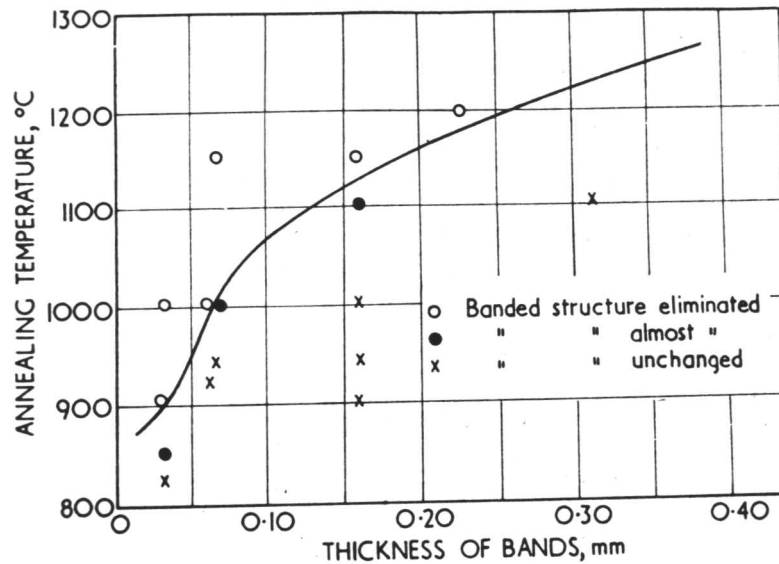


Fig. 2.7: Relationship between thickness of bands and reheating temperature (after Thompson and Willows<sup>[25]</sup>).

It is clear from figure 2.7 that there is a correspondence between the temperature required for the removal of the banded structure and the width of the bands. Since the homogenization time in a thermal treatment is proportional to the square of the dendrite arm spacing<sup>[26]</sup>, homogeneity is favoured by a short local solidification time. This time is defined as that between the initiation and completion of solidification at a given location in the ingot, and is inversely proportional to the average cooling rate at that location. Weinberg and Buhr<sup>[27]</sup> reported that the distortion of the dendritic structure by hot working had little effect on the rate of homogenization of microsegregation in the AISI 4340 alloy steel composition. Inoculation with certain elements,

\* Overheating means heating a metal or alloy to such a high temperature that its properties are impaired. When the original properties cannot be restored by further heat treating, by mechanical working, or a combination of working and heat treating, the overheating is known as burning.

e.g. calcium<sup>[28]</sup>, is sometimes employed to alter the ratio of dendrite arms to that of interdendritic spaces, although there is no change in the chemical composition of the dendrites.

Cox *et al.* <sup>[29]</sup> found that while heating sections of small laboratory-cast ingots of Fe-0.02C-0.25Mn-0.07Si-18.1Ni-5.85Mo-8.02Co-0.33Ti-0.005Al wt. % at 1232°C, the initial rate of homogenization is rapid, and may be sufficient to preclude the formation of reverted austenite during aging at 482°C. The rate later decreases to such an extent that complete homogenization by thermal treatment alone becomes impractical. Heating at 1200°C had a beneficial effect on the strength, ductility, and toughness of cast maraging steel. Hot rolling of a 120mm thick ingot section to 15mm thick plate affected a reduction of microsegregation similar to that obtained by heating an ingot at 1200°C for 4 hours, but resulted in even greater increases in ductility and toughness. This may be due to the enhancement of diffusion during mechanical working which considerably accelerates homogenization<sup>[30]</sup>. During plastic deformation, the movement and interactions of dislocations can result in the formation of vacancy defects. In so far as diffusion rate depends on vacancy concentration, mass flow will increase with high concentration of vacancies. The extent of this homogenization would be expected increase with increasing deformation, and should depend on the magnitude and distribution of the initial segregated solute.

#### 2.4 Segregation and the Properties of Materials

Segregation affects the basic materials parameters such as interfacial energies, self-diffusivity and the morphology of the interfaces. The effect of banding on the mechanical properties of steels is usually considered to be detrimental, although, it is often the case that no marked improvement in properties can be obtained with less heterogeneous structures. According to Jaczak *et al.* <sup>[22]</sup>, comparison of the longitudinal and transverse tensile properties of banded and of homogenized Fe-0.42C-0.72Mn-0.29Si-0.82Cr-1.74Ni-0.25Mo wt. % steel showed that only the transverse ductility was improved by homogenization, but even then the improvement was not commercially significant. Conversely, homogenization of through-the-thickness tension specimens of steel plate, (containing 1.47wt. % Mn, 0.21wt. %C) increased the strength by as much as 10% and the tensile ductility by at least a factor of 2.0, while the reduction in area was increased from 2.5 to 8.5 times by the homogenization<sup>[31]</sup> (Fig. 2.8).

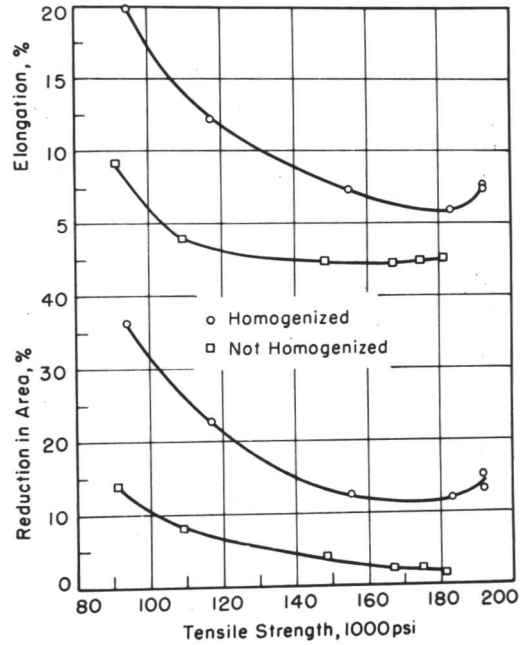


Fig. 2.8: Homogenized specimens showed improved strength and tensile ductility as compared to inhomogeneous (after Schwartzbart<sup>[31]</sup>).

Wilms<sup>[32]</sup> used commercial 50mm thick hot-rolled mild steel (Fe-0.22C-0.92Mn-0.07Si-0.012P-0.017S wt. %) to show that heterogeneity resulted in marked anisotropy, particularly with regard to impact properties and the tensile ductility. Similarly, Salmon Cox<sup>[29]</sup>, found that banding resulted in directional differences in plane-strain fracture toughness<sup>♣</sup>. The highest fracture toughness was obtained when the crack plane and direction were oriented normal to the plane of banding, and the lowest occurred when both the crack plane and the crack direction were parallel to the plane of bands. In the former case it was noticed that the fracture frequently detoured abruptly from its main course when it encountered segregation bands normal to the crack plane and propagation direction. Thus, segregation bands appeared to act as small internal crack arrestors, which tended to impede and divert the main crack and forced it to follow

♣ The plane-strain condition represents the more severe stress state in a crack opening mode when a tensile stress is applied in a direction normal to the faces of the crack. Plane-strain values of critical stress intensity factor are valid material properties, independent of specimen thickness, to describe the fracture toughness of strong materials. A stress intensity factor is a convenient way of describing the stress distribution around a flaw<sup>[33]</sup>.

a less direct path. This resulted in an increase in the measured fracture toughness of the material (Fe-0.013C-0.083Mn-0.069Si-18.1Ni-4.60Mo-7.71Co-0.47Ti-0.06Al wt. %) for this particular specimen orientation. However, it is important that the banding alone should not be considered when deciding the directionality of mechanical properties, since non-metallic inclusions have much greater effects. The inclusions not only act as regions of weakness but, depending on their shape relative to the test direction, can act as stress concentrators in the same way as a notch or crack. It has often been observed that notch ductility is lowest when the fracture runs parallel to the major axis of elongated inclusions<sup>[34]</sup>. It is important to recognize that satisfactory results may not be obtained simply by reducing the overall number or volume fraction of inclusions, unless the segregation of inclusions is also avoided. It has often been shown that anisotropy can be reduced by a high-temperature homogenizing treatment which reduces segregation and spheroidizes the inclusion stringers. However, this is generally an impractical solution due to the accompanying disadvantages such as oxidation and grain growth. Grange<sup>[35]</sup> developed a short-time, high-temperature treatment that eliminated ferrite-pearlite banding without markedly changing the shape of the inclusions, allowing him to compare the effects of inclusions in one steel in the banded and unbanded condition. When many elongated inclusions were present, removal of banding did little to improve transverse ductility. In the absence of inclusions removal of banding improved transverse ductility (reduction of area in a tensile test). Menter<sup>[36]</sup> performed hot notch tensile tests on specimens from segregated and unsegregated billets of En31 and confirmed the poor hot ductility associated with the former (Fig. 2.9).

Grange<sup>[35]</sup> realized that a few percent of martensite in banded steel is concentrated in relatively few bands, whereas when banding is removed, the same amount of martensite will be present as randomly dispersed small particles. The Hoggart<sup>[30]</sup>, showed that a large and rapid plastic deformation of an inhomogeneous material may give rise to the following effects:

- (a) stress gradients or discontinuities,
- (b) interfacial stresses,
- (c) crack or cavity formation,
- (d) inhomogeneity of deformation,

- (e) structural inhomogeneity,
- (f) residual stresses.

A shear stress on a material may cause plastic flow, tensile fracture, or shear fracture, but, in an inhomogeneous material, fracture in one component or portion of the material may occur before it commences to deform plastically. If the strain in a material is homogeneous, the stress field for a homogeneous material is uniform; but this is not the case for an inhomogeneous material as the stress to cause a particular strain depends on the “stiffness”, that is, the resistance to deformation of the material. Because the stress field in an inhomogeneous material must vary, stress gradients will occur and, if the inhomogeneity is discontinuous, a stress discontinuity will occur at the boundary so that interfacial stresses are generated. For a given strain, the magnitudes of the stress gradients, discontinuities or interfacial stresses depend on the stress differences and also on the relative sizes of the inhomogeneous regions.

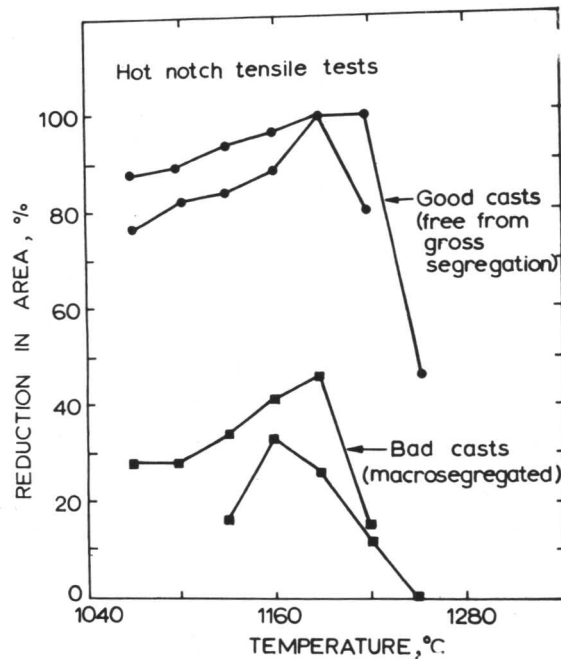


**Fig. 2.9:** Comparative hot ductility of segregated and unsegregated casts of En31 steel shown by the reduction in area during hot notched tensile test (after Menter<sup>[36]</sup>).

Solute segregation in the weld can lead to variations in mechanical properties throughout the weldment and also to the occurrence of a range of weld metal defects including porosity and solidification cracking. It can effect the strength and response of a non-transformable weld deposit to post weld heat treatment, or where solid-state transformation occurs after solidification, can alter the form of the final microstructure of the weld bead. Under particular welding conditions and with particular consumables, low- and high-carbon martensites and bainitic carbides form in groups of islands along the prior solidification boundaries. This produces a marked decrease in as-welded impact strength<sup>[37]</sup>. Moreover, there is a pronounced tendency for alloying and impurity elements to segregate to the weld centre line where the columnar grains growing from each side impinge, which in turn may produce hot tearing as a result of low-melting eutectics between the dendrite arms.

## 2.5 Heterogeneity and Phase Transformations

Austenite decomposition kinetics are affected by numerous factors, including chemical free energy changes produced by alloy combinations, the influence of alloying elements on the solubility of carbon in  $\gamma$ , the morphology and type of carbides that precipitate and their spacing, the changes occurring in the composition of the  $\gamma$  as ferrite forms during the bainite transformation, the effects of dislocations created during phase transformations, and probably other factors that are not as obvious. Small changes in chemical composition can vary the kinetics of transformations, as well as, the kind and volume fractions of transformation products. In mild and low alloy steel weld metal, a relationship is clearly apparent between the segregation associated with the extended cellular-dendritic growth characteristic of these materials and the formation of low-temperature transformation products and, in particular, low- and high-carbon martensites<sup>[37,38]</sup>. Davenport<sup>[39]</sup> determined the isothermal transformation curves of three different steels that showed banding behaviour. The isothermal transformation curves of these steels in both the homogenized and unhomogenized conditions are shown in figures 2.10-2.12.

For homogeneous alloys, the time interval between the beginning and end of transformation was appreciably smaller than for the corresponding heterogeneous alloys. For the unhomogenized material, the transformation start curves should be representative

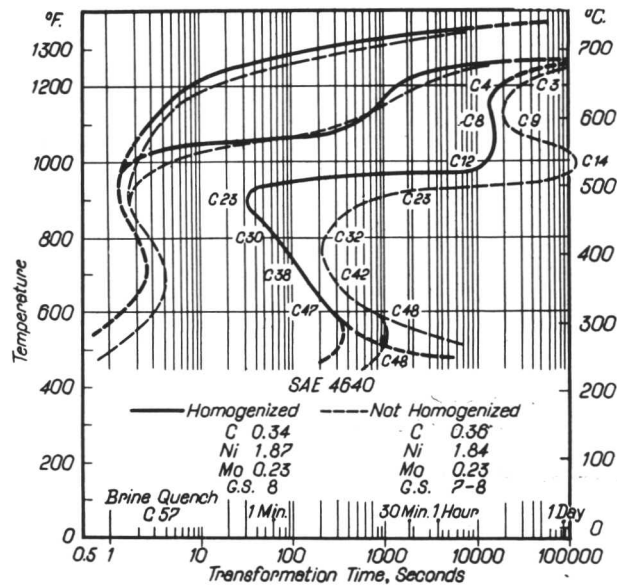


Fig. 2.10: Comparative isothermal transformation curves for S.A.E. 4640 (Fe-0.36C-0.63Mn-0.19Si-1.84Ni-0.06Cr-0.23Mo wt. %) before and after homogenization (after Devenport<sup>[39]</sup>).

of only the solute-depleted regions, while the transformation finish curve should be representative of only the high alloy solute-enriched regions.

Grange<sup>[35]</sup> observed the effect of banding in Fe-0.25C-1.5Mn wt. % steel on transformation of austenite. His results are summarized in figure 2.13. At all temperatures, transformation began slightly sooner in the steel without banding although no explanation is given for this. In fact, the primary phase to solidify in that investigation<sup>[35]</sup> was  $\gamma$  while in Davenport's investigation the primary phase was  $\delta$ . He also observed, in agreement with Davenport<sup>[39]</sup>, that above about 595°C this overall trend was reversed and completion was retarded in the steel without banding.

Farrar<sup>[40]</sup> has shown that in austenitic stainless steels the transformation at service temperature is strongly dependent on the original segregation of Cr, Mo and Ni in the as-welded condition. Depending upon the localised segregation within the  $\delta$ -ferrite laths they can exist in different parts of the Fe-Cr-Ni ternary phase diagram. If the initial segregation values allow the material to exist in the  $\delta + \gamma + \sigma$  phase field then the transformation is slow and the bulk of the ferrite is converted to carbides. but if

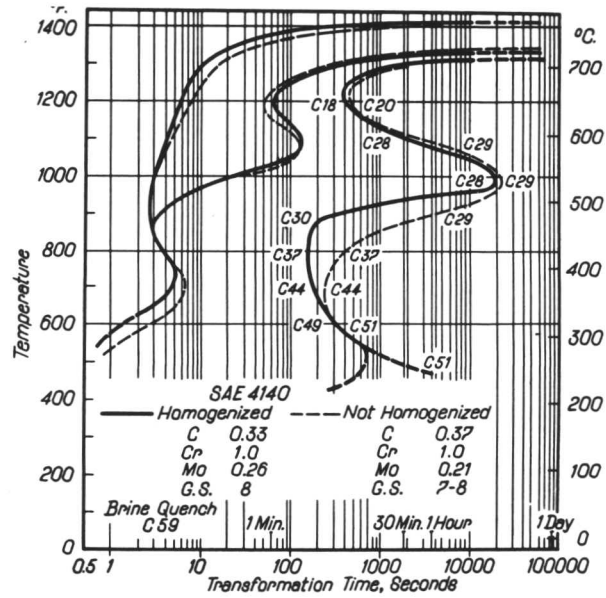


Fig. 2.11: Comparative isothermal transformation curves for S.A.E. 4140 (Fe-0.37C-0.77Mn-0.15Si-0.04Ni-0.98Cr-0.21Mo wt. %) before and after homogenization (after Devenport<sup>[39]</sup>).

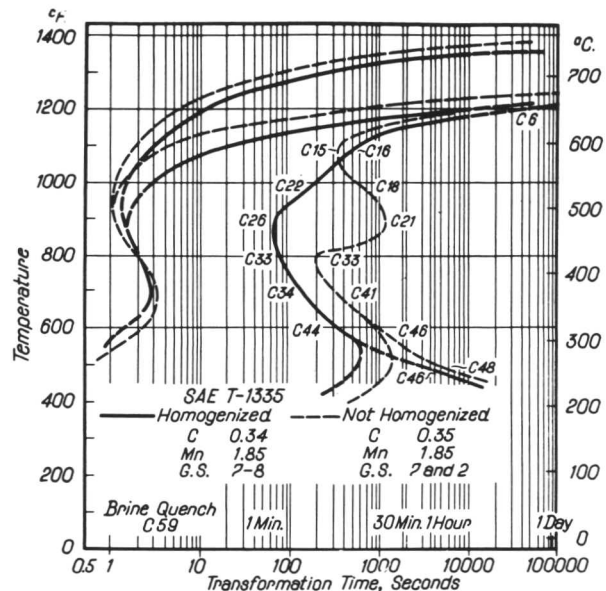
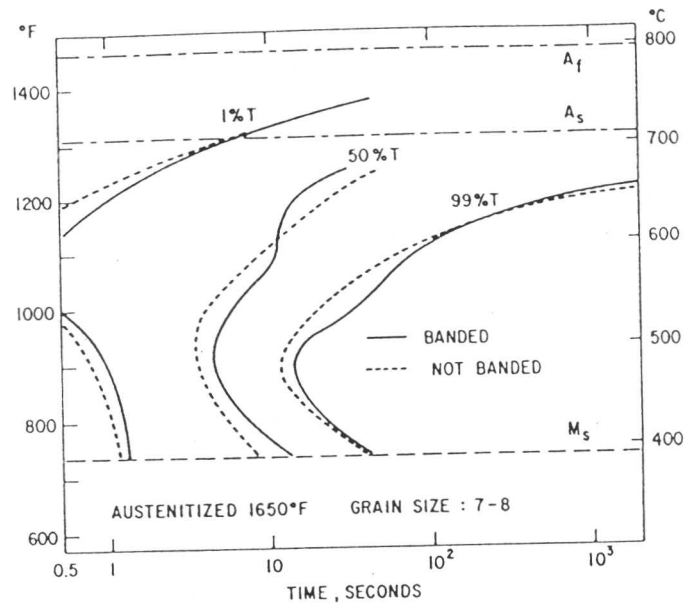


Fig. 2.12: Comparative isothermal transformation curves for S.A.E. T-1335 (Fe-0.35C-1.85Mn-0.19Si wt. %) before and after homogenization (after Devenport<sup>[39]</sup>).



**Fig. 2.13:** Effect of banding on isothermal transformation of austenite in Fe-0.25C-1.5Mn wt. % steel (after Grange<sup>[35]</sup>).

the material exists in the  $\gamma + \alpha$  phase field the transformation is rapid and the majority of the ferrite is converted to  $\sigma$  phase. Alfred Goldberg<sup>[41]</sup> found the development of martensite in a heterogeneous maraging steel to occur by the formation of layers as the transformation progressed. This layer formation which has been shown to be responsible for the anisotropic transformation strains, was attributed to the presence of banded segregation which caused the transformation to occur along layers in the parent phase. This was particularly evident for the austenite to martensite transformation which continued to completion by the lateral growth of these layers. The layer structure was revealed by interrupting the austenite to martensite transformation during cooling, reheating to age the martensite that has formed, and then allowing to cool to ambient temperature to complete the transformation of the residual austenite to unaged martensite. Wu *et al.* <sup>[34]</sup> have also mentioned that the ferrite-pearlite banding can be eliminated apparently when the cooling rate is higher than a critical value. The critical cooling rate was found to be inversely proportional to the square of interband distance. On cooling below this critical rate, the strength of steel increases rather rapidly with increasing cooling rate. At higher cooling rates, the strengthening effects are less pronounced.

The extent to which segregation affects the final microstructure is also determined by the austenite grain size and cooling rate through transformation. The incidence of banding may be related to the local effects of the segregants on ferrite nucleation and carbon diffusion. Phosphorus contributes to ferrite banding by raising the temperature of ferrite formation, but since nucleation is delayed, the effect is suppressed by fast cooling rates. An austenite grain structure coarse in proportion to the segregant distribution pattern minimizes banding at a given cooling rate by providing ferrite nucleation sites which traverse segregated and unsegregated regions. The metallographic method of estimating the progress of transformation is particularly sensitive to such inhomogeneity in composition as one microscopic area in a specimen frequently showing almost complete transformation while an adjacent area may scarcely show even the beginning of transformation. Such a state of affairs makes estimation of the progress of transformation, for the steel as a whole, very difficult indeed. For heterogeneous steels, it is not obvious how the maximum volume fraction of ferrite that can be obtained by isothermal transformation in the  $\alpha + \gamma$  phase field should differ from the corresponding maximum volume fraction of ferrite obtainable in a homogeneous steel of the same composition. There is experimental evidence<sup>[42]</sup>, that the maximum volume fraction of allotriomorphic ferrite obtained by prolonged isothermal transformation in a heterogeneous steel does not vary linearly with the average carbon content of the steel concerned. This implies that the lever rule is not valid for heterogeneous steels. Bhadeshia<sup>[43]</sup> looked into the effect of chemical heterogeneity on the formation of allotriomorphic ferrite by representing the banding as a composition wave of triangular shape and wavelength  $\lambda$  at constant amplitude. He showed that the final volume fraction of  $\alpha$  obtained at any temperature is independent of  $\lambda$ . However, while comparing the homogeneous and heterogeneous materials, we should be more concerned with the amplitude of the wave representing the variation of composition. Let wave A be represent the Mn concentration gradient in a heterogeneous material, and another wave B of smaller amplitude that for a relatively less heterogeneous material. Notice that the mean composition in the two situations are identical. This is illustrated in the Fig. 2.14, with the coordinate Z defined to be normal to the plane of constant composition in the specimen, that is normal to the plane of the diagram. Z is normalised to have a value of unity, equivalent to the total length of the specimen in the Z direction.

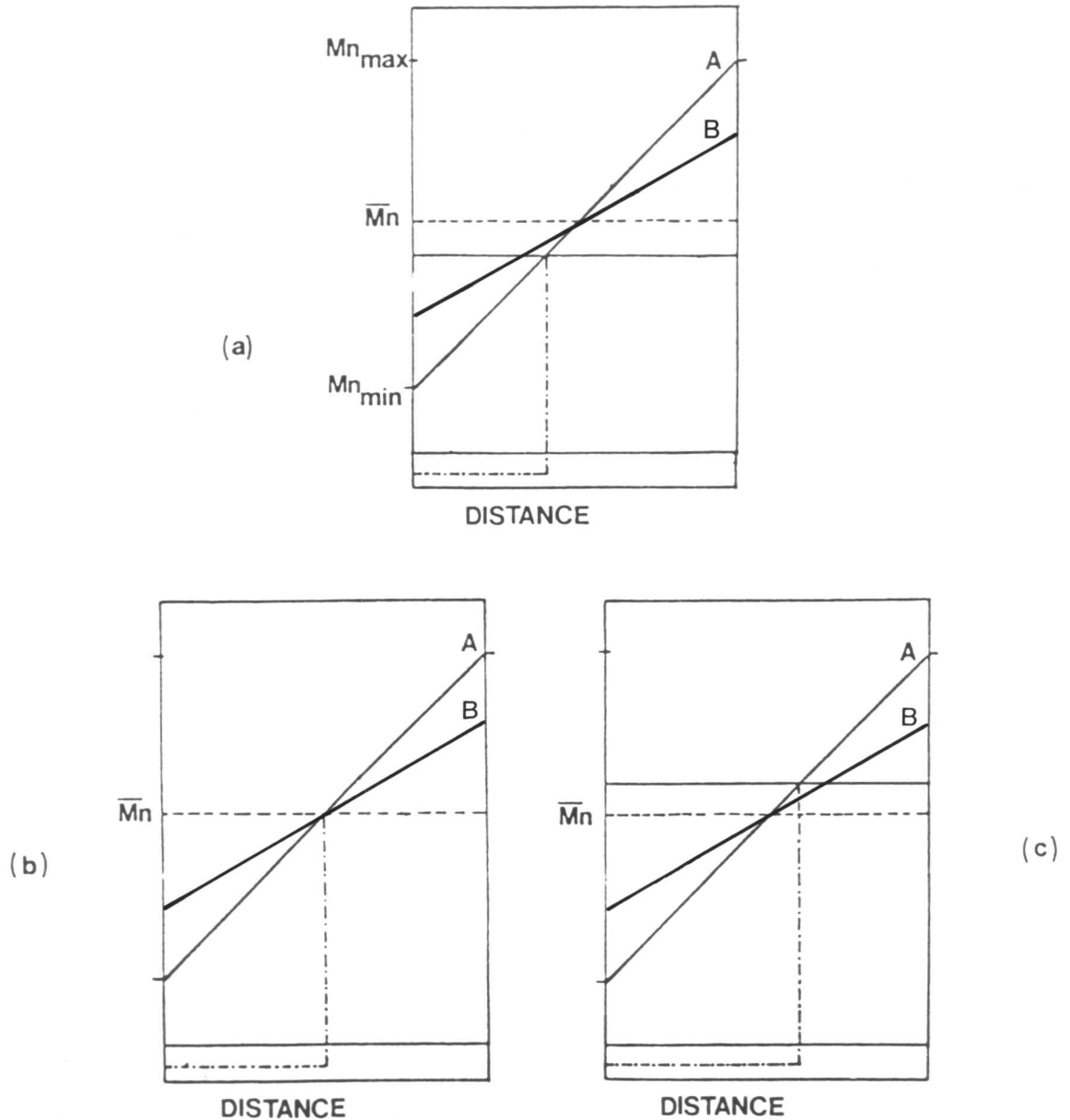


**Fig. 2.14:** Simulation of banding. The co-ordinate  $Z$  is defined to be normal to the planes of constant composition and is normalised with respect to the specimen length in the  $Z$ -direction. The curves  $A$  and  $B$  represent  $Mn$  concentration gradients in the banded steel. Vertical dotted lines show the volume fraction of ferrite represented by the position of interface for the two composition waves. Three different positions of the interface are shown in the figure:

- (a) when  $Mn < \bar{Mn}$ ,
- (b) when  $Mn = \bar{Mn}$ ,
- (c) when  $Mn > \bar{Mn}$ .

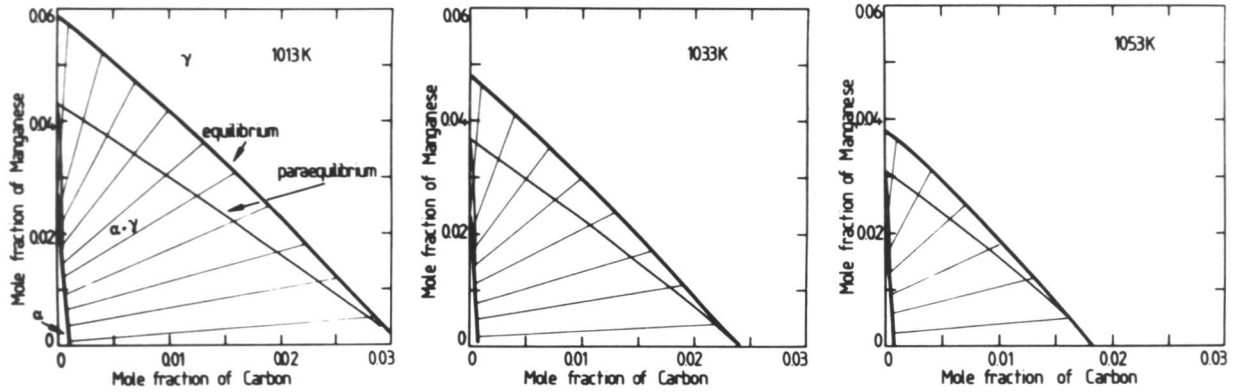


**Fig. 2.15:** Calculated isothermal sections of the Fe-Mn-C phase diagram, including the equilibrium and paraequilibrium phase boundaries. The tie-lines are for the equilibrium case, since those for paraequilibrium are all nearly parallel to the horizontal axis (after Bhadeshia<sup>[43]</sup>).

The formation of ferrite is expected to cease when  $x_\gamma = x_\gamma^{\gamma\alpha}$ . For the heterogeneous alloy under consideration,  $x_\gamma^{\gamma\alpha}$  varies with the position of the interface, since the Mn level also varies with  $Z$ .  $x_\gamma^{\gamma\alpha}$  is therefore a function of  $V$  and the condition for the reaction to cease may be written as:

$$x_\gamma^{\gamma\alpha}\{V\} = x_\gamma\{V\} \quad (2.9)$$

Where  $x_\gamma^{\gamma\alpha}$  and  $x_\gamma$  are implied to be function of  $V$ , by using the curly brackets. The two sides of this equation can be separately evaluated (using Fig. 2.15 and equation 2.8) and each plotted as a function of  $V$ , as shown in Fig. 2.16, where the calculations are carried out for steels with three different carbon concentrations, and for isothermal transformation at three different temperatures in the  $\alpha + \gamma$  phase field.

Curves such as 'ab' represent  $x_\gamma^{\gamma\alpha}\{V\}$  and the curves 'cd' represent  $x_\gamma\{V\}$ . Each intersection is a solution to equation 2.9, and gives a value of the Mn concentration at the position where the interface stops is  $[0.8 + (1.2 - 0.8)V_{ht}]$  since  $Mn_{\min}$  and  $Mn_{\max}$  (see figure 2.14) were taken to be 0.8 and 1.2 wt. % respectively. Each open circle in figure 2.16 represents the value of  $V_{hm}$  for a homogeneous steel containing 1.0 wt% Mn which is equal to the mean Mn level,  $\overline{Mn}$ , of the heterogeneous steel. To note the

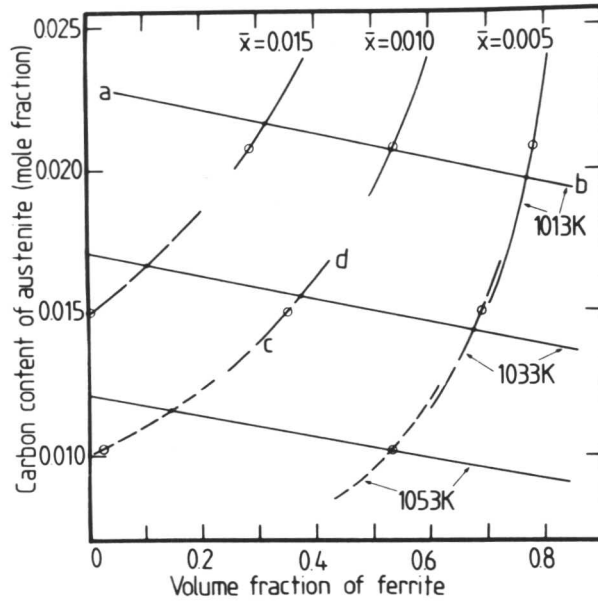


**Fig. 2.16:** Plot to determine the solution of equation (after Bhadeshia<sup>[43]</sup>).

difference between the transformation behaviour in homogeneous and heterogeneous steels, each open circle should be compared with the nearest intersection between curves of type 'ab' and 'cd'. This gives the corresponding values of  $V_{hm}$  and  $V_{ht}$ . It is evident from the above discussion that there are circumstances when  $V_{ht} > V_{hm}$ , and also cases where  $V_{ht} < V_{hm}$ . The former occurs when the interface stops at a point where the Mn level is less than  $\overline{\text{Mn}}$  and the latter when this Mn level is greater than  $\overline{\text{Mn}}$ . When heterogeneous steels are heat-treated at relatively large under coolings, such that the volume fraction of ferrite obtained is high enough to allow the transformation interfaces to stop at points where  $\text{Mn} > \overline{\text{Mn}}$ , the actual volume fraction of  $\alpha$  obtained will be less than that expected for homogeneous alloy. There will be no difference in  $V_{ht}$  and  $V_{hm}$  when Mn concentration at the interface equals  $\overline{\text{Mn}}$ . The linear variation of  $(1 - V_{hm})$  with  $\bar{x}$  implied by the lever rule will clearly not be valid for heterogeneous steels;  $(V_{ht} - V_{hm})$  depends on the absolute value of  $V_{ht}$ , which is in turn a function of  $\bar{x}$ . For any particular temperature, higher carbon steels lead to the formation of lower quantities of  $\alpha$  before reaction ceases, and the interface is then more likely to stop at a position where  $\text{Mn} > \overline{\text{Mn}}$ . This would lead to a higher than expected quantity of  $\alpha$  so that the curve  $(1 - V_{ht})$  versus  $\bar{x}$  would tend to have a decreasing positive slope with increasing  $\bar{x}$ , in agreement with the work of Speich and Miller<sup>[42]</sup>.

Gretoft *et al.* [45] presented a modified computer model for the prediction of microstructure in low alloy steel weld deposits to account for the presence of solidification-induced alloying element segregation. The new model was tested on Fe-Mn-Ni-Si-C alloys and the results indicate that segregation can significantly increase the amount of allotriomorphic ferrite in the microstructure by making its nucleation relatively easy. It is because the driving force for  $\gamma$  to  $\alpha$  transformation is the highest in the solute depleted regions where  $\alpha$  nucleation should first occur. In these circumstances, the major influence of segregation should be to raise the temperature at which  $\alpha$  first forms. For given cooling conditions, the  $\alpha$  then has more time to grow and the heterogeneous alloy should therefore have a higher volume fraction of  $\alpha$ . This is correct if the first phase to solidify is  $\delta$ , since the  $\delta/\delta$  boundaries ( where the last solute-rich liquid solidifies) are solute-rich. On further cooling, allotriomorphic  $\gamma$  nucleates at the  $\delta/\delta$  boundaries and when the  $\delta$  to  $\gamma$  reaction finishes, many of the  $\gamma/\gamma$  columnar-grain boundaries ideally lie along the centre of the prior  $\delta$  grains; the solute-depleted regions will therefore be at such  $\gamma/\gamma$  boundaries (Fig. 2.17). If the first phase to solidify is  $\gamma$  on the other hand, then solute segregation should make  $\alpha$  nucleation more difficult.

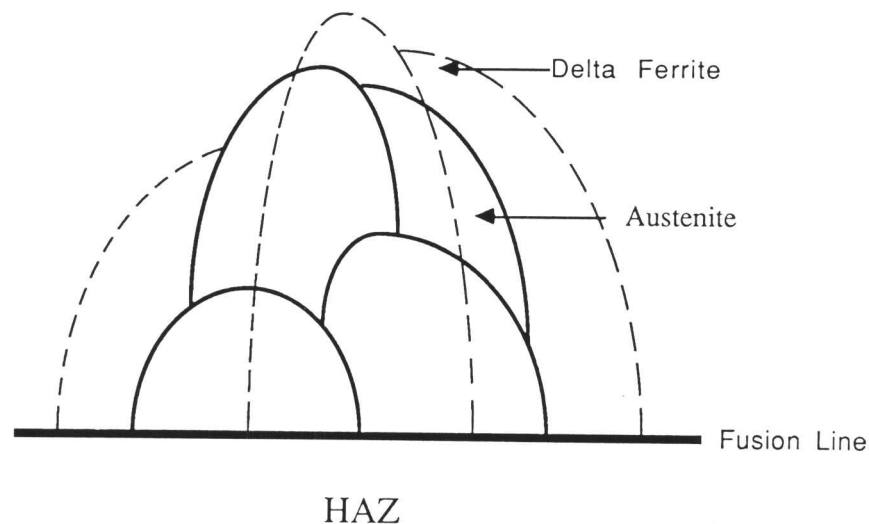


**Fig. 2.17:** Schematic illustration of austenite grains crossing primary delta ferrite grain boundaries.

### 2.5.2 Cooling Rate and Inhomogeneity

Collins<sup>[46]</sup> observed that by increasing cooling rate not only the microstructure is refined but the temperature range over which most of the transformation occurs is narrowed producing a more uniform microstructure instead of ferrite-pearlite banding. Such microstructural banding is due to inhomogeneous nucleation of ferrite and is usually attributed to segregation of Mn and other elements, which leads to enhanced ferrite nucleation in the Mn-depleted regions and low temperature products in the Mn rich-regions. Regardless of the origin of the initial nucleation rate inhomogeneity, the diffusion of carbon ahead of the  $\gamma/\alpha$  interface into regions at which nucleation occurs at lower temperature further suppresses the transformation temperature in this region. Increased cooling rate reduces the time interval between nucleation at the most potent nucleation sites and the onset of transformation at less active sites. Consequently, the extent of ferrite growth from the most potent nucleation sites and the accompanying carbon segregation is reduced. Nucleation may occur at less active sites before carbon level begins to rise. Thus, with accelerated cooling rates, ferrite nucleation occurs more uniformly throughout the steel and the development of carbon rich regions or bands is reduced or eliminated. Tamehiro *et al.* <sup>[47]</sup> have shown (Fig. 2.18) that the carbon distribution of the accelerated cooled plate is fairly uniform compared with that of the controlled rolled plate, though the concentration of Mn, P and other elements is the same for both plates.

The enrichment of carbon in the segregated zone of the controlled rolled plate occurs due to a lower cooling rate after rolling, because the segregation of Mn and other elements retards  $\gamma$  to  $\alpha$  transformation in the segregated zone, thus facilitating diffusion of carbon from the non-segregated area to the segregated zone. In the case of the accelerated cooled plate with a higher cooling rate, however, such a diffusion of carbon is suppressed and a banded microstructure disappears<sup>[47]</sup>, as illustrated in Fig. 2.19.

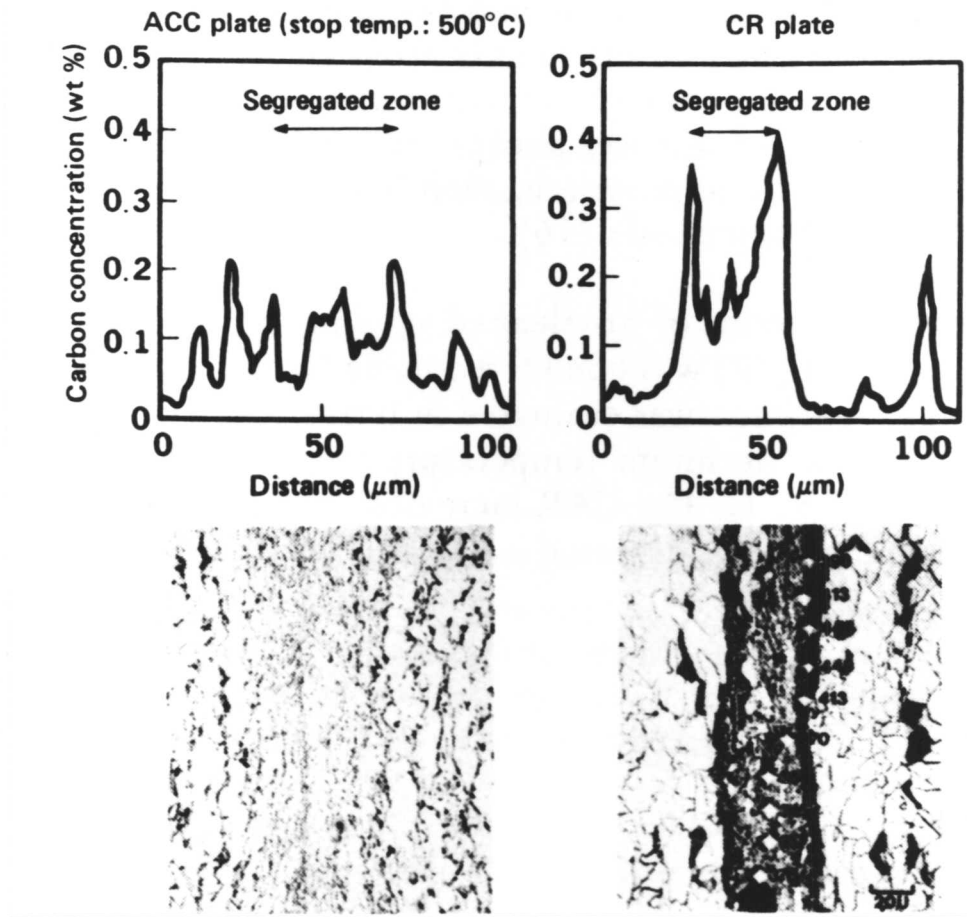


Fig. 2.18: Distribution of carbon concentration in segregated zones of an accelerated cooled plate and a controlled rolled plate (after Tamehiro *et al.* [47]).

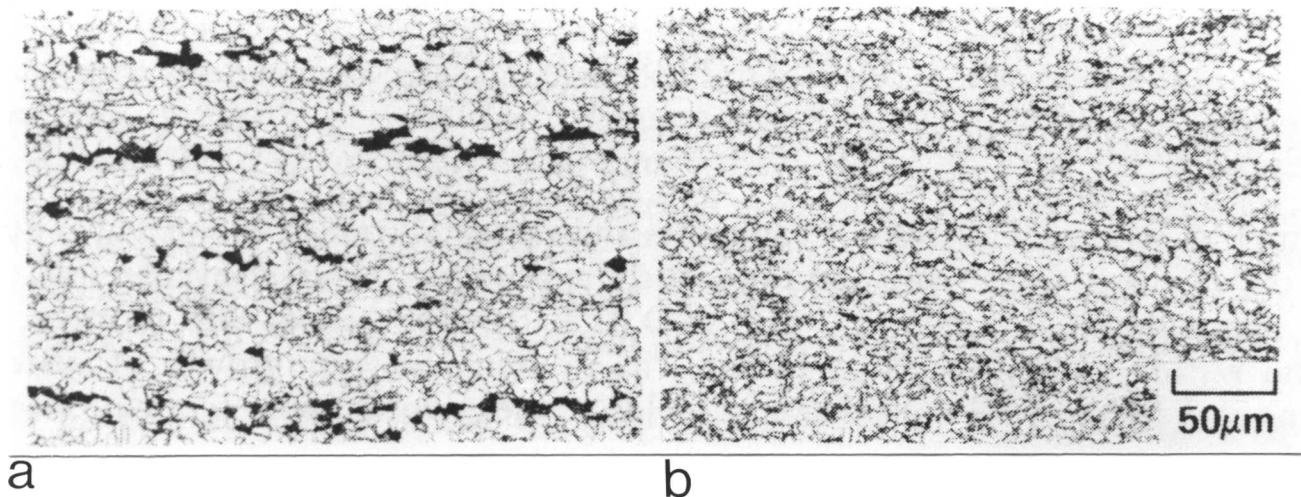


Fig. 2.19: Microstructural change of plate with accelerated cooling after controlled rolling (after Tamehiro *et al.* [47]).

(a) Controlled rolled plate.

(b) Plate after accelerated cooling.

## REFERENCES

1. K. Easterling: *Introduction to the Physical Metallurgy of Welding*, p. 59, Butterworths and Co. (publishers) Ltd., 1983.
2. D. A. Porter and K. E. Easterling: *Phase Transformations in Metals and Alloys*, p. 208, Van Nostrand Reinhold (UK) Co. Ltd., 1981.
3. T. W. Miller: *M. S. Thesis*, Rensselaer Polytechnic, Troy, New York, 1867.
4. L. Bäckerud and L. M. Liljenvall: *J. Inst. Metals*, 1972, vol. 100, p. 366.
5. D. J. Hebditch and J. D. Hunt: *Metall. Trans.*, 1974, vol. 5, p. 1557.
6. M. C. Flemings and G. Nereo: *Trans. AIME*, 1967, vol. 239, p. 1449.
7. M. C. Flemings and G. Nereo: *Trans. AIME*, 1968, vol. 242, p. 41.
8. M. C. Flemings and G. Nereo: *Trans. AIME*, 1968, vol. 242, p. 50.
9. K. Hirano, M. Cohen and B. L. Averbach: *Acta Met.*, 1961, vol. 9, p. 440.
10. J. Askill: *Tracer Diffusion Data for Metals, alloys and Simple Oxides*, Plenum Data Corporation, 1970.
11. W. Batz, H. W. Mead and C. E. Birchenall: *Trans. AIME*, 1952, p. 1070.
12. H. D. Brody and M. C. Flemings: *Trans. AIME*, 1966, vol. 236, p. 615.
13. H. Fredriksson: *Scand. J. Metall.*, 1976, vol. 5, p. 27.
14. M. C. Flemings: *The Solidification of Metals*, p. 370, The Iron and Steel Institute, London, 1968.
15. J. S. Kirkaldy, B. A. Thomson and E. A. Beganis: *Hardenability Concepts With Application to Steels*, p. 82, AIME, USA, 1977.
16. H. Finiston and T. Fearnough: *J. I. S. I.*, 1951, vol. 69, p. 6.
17. B. V. Zakharov: *Russ. Cast. Prod.*, 1969, p. 415.
18. P. G. Bestien: *J. I. S. I.*, 1957, vol. 187, p. 281.
19. A. A. B. Sugden: *PhD. Thesis*, University of Cambridge, UK, 1988.
20. H. D. Brody: *Trans. of Metall. Soc. AIME*, 1966, vol. 236, p. 624.
21. M. C. Flemings *et al.* : *Trans. AIME*, 1968, vol. 242, p. 41.
22. C. F. Jatzcak, D. J. Girardi and E. S. Rowland: *Trans. A. S. M.* , 1956, vol. 48, p. 279.
23. J. S. Kirkaldy, V. D. Forstmann and R. J. Brigham: *Cand. Metall. Quart.*, 1962, vol. 1, p. 59.

24. J. D. Lavender and F. W. Jones: *J. I. S. I.*, 1949, vol. 163, p. 14.
25. F. C. Thompson and R. Willows: *J. I. S. I.*, 1931, p. 151.
26. D. Dulieu and I. G. Davies: *Metals Technology*, 1975, p. 178.
27. F. Weinberg and R. K. Buhr: *J. I. S. I.*, 1969, vol. 207, p. 1114.
28. N. A. Manyak: *Steel in the USSR*, 1986-88, p. 292.
29. P. H. S. Cox, B. G. Residorf and G. E. Pellissier: *Trans. Metall. Soc. AIME*, 1967, vol. 239, p. 1809.
30. J. S. Hoggart: *J. Aust. Inst. Met.*, 1969, vol. 14, p. 10.
31. H. Schwartzbart: *Trans. A. S. M.*, 1952, vol. 44, p. 845.
32. G. R. Wilms: *J. Aust. Inst. Met.*, 1973, vol. 18, p. 47.
33. G. E. Dieter: *Mechanical Metallurgy*, p. 353, McGraw-Hill Inc., 1986.
34. W. Chuen-Taur and P. Yeong-Tsuen: *Processing, Microstructure and Properties of HSLA Steels*, Conf. Proc., TMS Minerals-Metals-Materials, Pittsburg, 1986.
35. R. A. Grange: *Metall. Trans.*, 1971, vol. 2, p. 417.
36. J. W. Menter: *J. I. S. I.*, 1971, p. 249.
37. J. G. Garland and P. R. Kirkwood: *International Institute of Welding Document*, IX-92-74, 1974.
38. J. G. Garland: *BSC Report*, Prod/500/1/73/A, 1973.
39. E. S. Davenport: *Trans. A. S. M.*, 1939, p. 837.
40. R. A. Farrar: *Stainless steels '84*, p. 336-342, Institute of Metals, London, 1985.
41. A. Goldberg: *Trans. A. S. M.*, 1969, vol. 62, p. 219.
42. G. R. Speich and R. L. Miller: *Trans. Metall. Soc. AIME*, 1979, p. 145.
43. H. K. D. H. Bhadeshia: *Scripta Metall.*, 1983, vol. 17, p. 857.
44. J. B. Gilmour, G. R. Purdy and J. S. Kirkaldy: *Metall. Trans.*, 1972, vol. 3, p. 1455.
45. B. Grefott, H. K. D. H. Bhadeshia and L. E. Svensson: *Acta Stereol.*, 1986, p. 365.
46. L. E. Collins, R. F. Knight, G. E. Ruddle and J. D. Boyd: *Accelerated cooling of steel*, p. 261, Conf. Proc., Metall. Soc. AIME, Pittsburgh, 1985.
47. H. Tamehiro, R. Habu, N. Yamada, H. Matsuda and M. Nagumo: *Accelerated cooling of steel*, p. 401, Conf. Proc., Metall. Soc. AIME, Pittsburgh, 1985.

## Chapter 3

### EXPERIMENTAL TECHNIQUE

#### 3.1 Materials

The materials used in this work are as follows:

- **300M** has a typical composition of was a low alloy steel (300M) containing Fe-0.45C-1.70Si-0.70Mn-1.90Ni-0.80Cr-0.40Mo-0.10V wt.%. During manufacture electrodes were produced from basic electric arc vacuum degassed steel, which were then vacuum arc remelted to 406 mm diameter ingot. The ingot was then annealed and forged on a precision forging machine to 135 mm square bar. The maximum forging temperature used was 1150 °C. It was then further annealed at 650/700 °C.
- **US83** and **US24** are of compositions Fe-0.20C-0.63Si-2.80Mn-0.04Ni-0.01Mo-1.10Cr wt. % and Fe-0.18C-0.75Si-1.98Mn-0.02Ni-0.01Mo-1.33Cr wt. % respectively. The steels were produced as electric furnace heats and continuously cast into 178 x 178 mm billets. These billets were reheated to 1232 °C , rolled to 22 mm diameter rods and air cooled. The steels are described as “air hardening” steels because of the mixed bainite/martensite/austenite microstructure which results after rolling and air cooling. These samples were produced by Inland Steel.
- **BS** is a badly segregated structural steel of average composition *Fe-0.17C-0.35Si-1.38Mn wt. %*.

#### 3.2 Heat-Treatment

The aim of this work was to study the differences in transformation behaviour between chemically heterogeneous and homogeneous steels. To produce homogeneous samples, some of the steels were annealed at 1300 °C for three days. A vacuum furnace was used for this heat-treatment. In some cases, specimens were sealed in silica tubes under a partial pressure of argon in order to prevent oxidation and decarburisation. The silica tube was flushed three times with argon in each case, before sealing. The temperature was in all cases measured, using a Pt/Pt13 wt. % Rh thermocouple, at the specific position in the tube furnace where the specimens were located.

### 3.3 Optical Microscopy

Optical microscopy was used to observe the heterogeneity of microstructure after a variety of heat treatments. The specimens were hot mounted in acrylic plastic, and ground on silicon carbide paper to a sufficient depth to remove any unrepresentative surface. They were then mechanically ground down to 1200 grade emery paper and finally polished with 6, 1 and  $\frac{1}{4}$  micron diamond pastes. Picral, sodium metabisulphite and 2% Nital were used as etchants for different purposes throughout this work. Photography was carried out using an Olympus camera fitted to an Olympus microscope.

### 3.4 Dilatometry

Transformation can be detected as it happens using precision dilatometry, which is capable of sensing volume or heat capacity changes during the course of phase transformations. For this purpose a high speed dilatometer (Theta industries) was used, fitted with a water cooled radio frequency furnace. Nickel plated specimens were used throughout to avoid decarburisation. Nickel plating was carried out in two stages, i.e. striking and plating. Striking was carried out in a solution made up of 250g nickel sulphate, 27ml concentrated sulphuric acid and water, amounting to one litre in all. The solution was used at 50 °C, with a current density of 7.75 mA/mm<sup>2</sup>, for three minutes. The plating solution consisted of 140g nickel sulphate, 140g anhydrous sodium sulphate, 15g ammonium chloride and 20g boric acid, made up to one litre with distilled water. The plating was carried out at 50 °C, with a current density of 0.4mA/mm<sup>2</sup> for fifteen minutes, to give a plate thickness of approximately 0.08 mm. A "Data-Trak Programme", which is a pre-programmed heating schedule, was used for heating the specimen to the austenitizing temperature. For isothermal studies, a manual temperature control device was used to quench the specimen from its austenitizing treatment temperature to the pre-set transformation temperature. Rapid quenching was achieved by flushing with He gas. Any change in length of the specimen is transmitted to the transducer and nominally magnified 10<sup>4</sup> times. The length transducer on the dilatometer was calibrated using pure platinum specimen of known thermal expansion characteristics. Data consisting of time, temperature and relative length change are collected on a floppy disc using a BBC microcomputer attached to the dilatometer. Both change in length and temperature were also monitored on a chart recorder which

moves at a pre-set speed.

### 3.5 Microhardness Testing

Microhardness measurements were made on polished and etched specimens using a Leitz hardness measuring digital eyepiece with the option of Vickers hardness tester to which a computer-counter-printer was attached. The indentation load applied for indentation was 0.981 N in each case. All the measurements were made at a suitable distance from the specimen edge. At least twenty readings were taken per specimen. In the case of heterogeneous specimens, measurements were made both along and across the segregation bands.

### 3.6 Microanalysis

Microanalysis experiments were carried out using energy dispersive X-ray analysis (interaction volume approximately  $4.5 \mu^3$ ) on a scanning electron microscope. The data obtained were analysed using the LINK microanalysis programme which corrects for the following effects:

- *Fluorescence i.e.*, photoelectric effect leading to secondary ionisation,
- *Atomic Number i.e.*, emitted X-ray intensity is affected by mass of sample penetrated by electrons, moreover, backscattering increases with increasing atomic number,
- *Absorption i.e.*, X-ray partially absorbed due to photoelectric effect.

### 3.7 Transmission Electron Microscopy

Philips EM300 and 400T electron microscopes were used for the examination of thin foils. The operating voltage was 100 kV and 120 kV respectively. Thin foil specimens were prepared for transmission electron microscopy from 0.25mm thick discs slit from specimens used in the dilatometric experiments. The discs were thinned down to 0.05mm by abrasion on silicon carbide paper and then electropolished in a twin jet electropolisher using a 5% perchloric acid, 25% glycerol and 70% ethanol mixture.

## Chapter 4

# THE BAINITE TRANSFORMATION IN CHEMICALLY HETEROGENEOUS 300M HIGH-STRENGTH STEEL

### 4.1 Introduction

300M is a medium carbon steel alloyed with several substitutional solutes and has a typical chemical composition Fe-0.45C-1.7Si-0.7Mn-1.9Ni-0.8Cr-0.4Mo-0.1V wt.%. The different alloying elements have many purposes<sup>[1-4]</sup>, but they all serve to enhance hardenability to such an extent that a 10cm diameter bar can be air cooled to a uniform martensitic microstructure. Molybdenum also helps to limit impurity-controlled temper embrittlement effects, and nickel has an intrinsic beneficial influence on the toughness of the martensite<sup>[1]</sup>. Vanadium serves to restrict austenite grain growth during the austenitising heat-treatment, usually carried out at a temperature not high enough to completely dissolve particles of vanadium carbides. The composition is in fact based on the popular “4340” steel which acquires its optimum strength and toughness in the quenched and tempered martensitic condition. The 4340 steel unfortunately suffers from tempered martensite embrittlement, in which the toughness goes through a minimum at a tempering temperature of  $\simeq 300$  °C. At low tempering temperatures the cementite particles are too fine to be detrimental. Although at high tempering temperatures they are relatively coarser, the yield strength is by then rather low so that the material can accommodate coarser particles. It is at the intermediate temperatures where the curve of toughness versus tempering temperature shows a minimum that there is an unfavourable combination of cementite particle size and yield strength. The 300M steel was designed to avoid this problem by increasing the silicon concentration to a level high enough to retard the coarsening of cementite, and hence to shift the toughness minimum to a higher tempering temperature. It can therefore be tempered at a relatively low temperature and hence avoid the large loss of strength associated with tempering at elevated temperatures<sup>[1-3]</sup>.

Both 4340 and 300M steel are best utilised in the quenched and tempered condition. When attempts are made to use 4340 steel in a bainitic condition, the toughness obtained is not impressive because of the coarse cementite particles associated with upper bainite in this medium carbon steel. On the other hand when 300M steel is

isothermally transformed to upper bainite, cementite does not readily precipitate and the microstructure then contains only bainitic ferrite and residual austenite\* at the isothermal transformation temperature. This is due to the high silicon concentration which severely retards the precipitation of cementite from the residual austenite. However, the toughness in the isothermally transformed 300M steel is still poor compared with that associated with tempered martensite, because some of the carbon-enriched residual austenite transforms to high-carbon, untempered martensite during cooling to ambient temperature. Furthermore, the austenite retained at ambient temperature is unstable to stress-induced martensitic transformation, a phenomenon which in this instance is detrimental since the energy absorbed by the transformation is inadequate to compensate for the brittle nature of the transformation product<sup>[5-8]</sup>.

If the mechanical stability of the residual austenite in isothermally transformed 300M steel could be improved, the resulting microstructure of just bainitic ferrite and stable retained austenite should have a good combination of strength and toughness, since the ultrafine-grained body-centered cubic (BCC) platelets of bainitic ferrite are then separated by tough and inherently more ductile films of stable face-centered cubic (FCC) austenite. It has been demonstrated that the structure of high-silicon bainitic steels can be optimised by using phase transformation theory<sup>[7-11]</sup>. If it is assumed that the growth of bainite is diffusionless, but that the carbon is partitioned into the residual austenite immediately after transformation, then the bainite reaction should stop when the carbon concentration of the residual austenite reaches the  $T_o$  curve on the phase diagram.

The  $T_o$  curve defines the locus of all temperatures at which austenite and ferrite of the same chemical composition have the same free energy (see for example<sup>[12]</sup>); hence, diffusionless growth of bainite is thermodynamically impossible if the carbon concentration of the austenite exceeds that given by the  $T_o$  curve at the appropriate transformation temperature. In fact, the growth of bainite is accompanied by a shape deformation which has to be accounted for in deciding the thermodynamic criteria for

---

\* Throughout this chapter, the term "residual austenite" refers to the austenite that exists at the reaction temperature during isothermal transformation to bainite, whereas the term "retained austenite" refers to the austenite which remains untransformed after cooling the specimen to ambient temperature.

growth. The  $T'_o$  curve, which also allows for the stored energy due to transformation (estimated to be about  $400\text{Jmol}^{-1}$  for bainitic ferrite<sup>[13]</sup>), gives the more appropriate condition for the formation of bainite. It will later also be necessary to consider the  $A'_{e3}$  curve, which is the paraequilibrium  $\alpha + \gamma/\gamma$  phase boundary. Note that much of the stored energy arises from the strain energy due to the invariant-plane strain shape change accompanying transformation. The calculation of the strain energy is carried out for an isolated plate which grows under purely elastic constraint. Plastic accommodation effects and elastic interactions between plates will in reality reduce the value of stored energy.

A more stable austenite is obtained if the  $T_o$  curve is shifted towards higher carbon concentrations<sup>[7,8]</sup>. The position of the  $T_o$  curve is determined by the thermodynamics of the BCC and FCC solid solutions, since it gives the locus of all temperatures where austenite and ferrite of the same composition have equal free energy. Hence, the microstructure of silicon steel can be controlled using the thermodynamic theory of the bainite transformation.

The concepts discussed above have been tested successfully for a range of high-strength steels<sup>[7-11]</sup>. However, the theory is strictly applicable only to chemically homogeneous steels. On the other hand, most commercial steels are to some extent chemically heterogeneous, and it is certainly common to observe a banded bainitic microstructure in isothermally transformed 300M steel. The purpose of the present work was to develop phase transformation theory to enable the prediction of the extent of bainitic transformation in chemically heterogeneous high-silicon steels. The work is a part of a general programme on modelling the development of microstructure in low-alloy steels.

## 4.2 Results and Discussion

Microanalysis was carried out on heterogeneous samples austenitised at  $950\text{ }^\circ\text{C}$  for  $10\text{min}$  and isothermally held at  $400\text{ }^\circ\text{C}$  until the transformation ceased. Light microscopy revealed a heavily banded microstructure consisting of (solute-depleted) regions which are predominantly bainitic, separated by bands of predominantly martensitic microstructure (Fig. 4.1a, b).

The microanalysis data are presented in Fig. 4.2 where the regions designated “matrix” were essentially untransformed at the isothermal transformation temperature and are seen to be significantly richer in substitutional alloy concentration. The range of concentration variation was found to be approximately 1.55-1.97Si, 0.56-0.89 Mn, 1.74-2.06 Ni, 0.35-0.88 Mo, 0.77-1.44Cr and 0.0-0.18 V, wt.%. Since the microanalysis technique draws information from an interaction volume which is about  $4.5\mu\text{m}^3$ , the actual variations in solute concentrations may be underestimated in the data of Fig. 4.2. An underestimation of this kind should lead to a large error in any attempt at calculating the nucleation rate of bainite in the heterogeneous samples, since the size of the nucleus is likely to be much smaller than the interaction volume. However, the main aim of the present work is to examine the *limiting* volume fractions of bainite obtained after prolonged isothermal transformation. Since the volume of a sheaf of bainite is expected to be much larger than the interaction volume, any error resulting from the spatial resolution of the microanalytical technique, in calculating the limiting volume fraction of bainitic ferrite should be negligible. Note also that it is not necessary to consider an inhomogeneous carbon distribution in the austenite at 950 °C since the diffusivity of carbon in austenite is very large at that temperature. This does, however, involve the approximation that during austenitisation, it is the concentration of carbon which is uniform throughout, instead of its activity. The latter is a function of the substitutional solute concentration, which in turn is not constant.

On the other hand, for dilute steels such as the 300M steel used here, it is unlikely that the concentration of carbon varies significantly within the austenite at 950 °C. This is verified by the uniformity of hardness data (Fig. 4.3) from fully martensitic specimens obtained by quenching into iced-brine following austenitisation at 950 °C for 10 mins. The load used for hardness testing was such that the indent size was less than about half the typical microstructural band width.

With the exception of silicon, all of the elements Ni, Mn, Mo, V and Cr are expected to retard the bainite reaction as illustrated in Fig. 4.4 which shows time-temperature-transformation (TTT) diagrams for hypothetical steels of composition similar to 300M, calculated using the method of Bhadeshia<sup>[14,15]</sup>. The effect of an excess addition of 1wt.% of each alloying addition is examined (for silicon, the excess addition is 2wt.%

in order to produce a discernable effect). Based on these data, it is expected that the solute depleted regions should transform first.

Fig. 4.5 shows a typical dilatometric plot of the change in relative specimen length as a function of temperature during cooling from the austenitising temperature to the lowest isothermal transformation temperature used in the present experiments. The linearity of the plot proves the lack of any transformation during the quench to the isothermal transformation temperature.

Isothermal transformation experiments were carried out over the temperature range 440-320 °C, for both the homogenised and as-received samples. Typical microstructures, as characterised using transmission electron microscopy are illustrated in Figs. 4.6 and 4.7. Carbide-free upper bainite was obtained in all cases except for transformation at 320 °C, where a small amount of lower bainite (Fig. 4.7) was also observed. As with the upper bainite obtained by transformation at higher temperature, austenite was also found between the subunits of lower bainite. Since the presence of lower bainite is not accounted for in the calculations; the carbide particles in the lower bainite in effect remove carbon from the system, the results of the theoretical analysis of the data obtained from the 320 °C experiments are treated with caution.

#### 4.2.1 Dilatometric Analysis

The results of isothermal transformation experiments are presented in Fig. 4.8 and supported by metallographic evidence (Fig. 4.9). As expected, the curves are all of sigmoidal shape, the extent of transformation reaching some maximum value, denoted by a maximum length change  $(\Delta l/l)_m$  on prolonged holding at the isothermal transformation temperature. The length change obtained in the dilatometric experiments can be related to the volume fraction of upper bainite  $V_b$  obtained as follows:

$$\frac{\Delta l}{l} = \frac{2V_b a_\alpha^3 + (1 - V_b) a_\gamma^3 - \bar{a}_\gamma^3}{3\bar{a}_\gamma^3} \quad (4.1)$$

where  $a_\alpha$  is the lattice parameter of ferrite at the transformation temperature, given by:

$$a_\alpha = a_o^\alpha [1 + e_\alpha (T - 25)] \quad (4.2)$$

and  $\bar{a}_\gamma$ , which is the lattice parameter of austenite of the alloy composition at the transformation temperature, is give by:

$$\bar{a}_\gamma = (a_o^\gamma + \Sigma c_i x_i) [1 + e_\gamma (T - 25)]. \quad (4.3)$$

In these equations,  $e_\alpha$  and  $e_\gamma$  represent the linear thermal expansivities of ferrite and austenite respectively,  $a_o$  is the lattice parameter of austenite in pure iron at 25 °C,  $x_i$  is the concentration of alloying element  $i$  and  $c_i x_i$  represents the change in  $a_o$  due to the addition of the alloying element to pure iron.  $T$  is the temperature in °C. Values of  $e_\alpha$ ,  $e_\gamma$  and  $a_o^\alpha$  are given by  $1.1103 \times 10^{-5} K^{-1}$ ,  $1.7951 \times 10^{-5} K^{-1}$  and  $0.28661 \pm 0.0001 nm$  respectively<sup>[16]</sup>. The coefficients  $c_i$  and the parameter  $a_o^\gamma$  is from the work of Dyson *et al.* [17].

After making the appropriate substitutions, the above equations can be solved to give the volume fraction of bainite (Table 4.1) and the carbon concentration of the residual austenite. In this way, the carbon concentration in the austenite at the point where isothermal transformation ceases can be calculated, and a comparison of such data for upper bainite, with the  $T_o$ ,  $T'_o$  and  $A'_{e3}$  curves, calculated for the chemical composition of the homogeneous alloy, is presented in Fig. 4.10.

If the growth of bainite is assumed to be diffusionless, and carbon is subsequently partitioned into the residual austenite, then in the absence of any other interfering reactions, the formation of bainite should cease when the carbon concentration of the residual austenite reaches somewhere between the limits defined by the  $T_o$  and  $T'_o$  curves. On the other hand if the bainitic ferrite does not form with any supersaturation of carbon then the reaction can in principle continue until the carbon concentration of the residual austenite reaches the paraequilibrium  $A'_{e3}$  phase boundary. It is evident from Fig. 4.10 that the experimental data support the conclusion that the growth of bainite is diffusionless, with the carbon being partitioned subsequently into the residual austenite. Fig. 4.11 illustrates a similar comparison for the as-received (heterogeneous) sample of 300M steel, which was isothermally transformed to upper bainite. In Fig. 4.11, the calculations of phase boundaries cover the range of chemical compositions detected experimentally. The results are again consistent with the hypothesis that the growth of bainite is diffusionless. The results show that 300M steel accurately exhibits the incomplete reaction phenomenon, which can be used to estimate theoretically the degree of transformation expected as a function of isothermal transformation temperature or in terms of the detailed alloy chemistry. They also show that fully bainitic microstructures cannot be obtained in 300M steel by any heat-treatment, since the final microstructure obtained at ambient temperature is always expected to be some

mixture of bainite, high-carbon untempered martensite and carbon-enriched retained austenite. This has implications in the interpretation of microstructure/property data.

A further examination of the experimental data (Figs. 4.8-12, Table 4.1) shows that the maximum degree of transformation obtained at any isothermal transformation temperature is higher for the homogenised samples when compared with the as-received steel. The exception is at very low undercoolings below the  $B_s$  temperature, where the degree of transformation is higher for the heterogeneous samples. The effect of chemical segregation in general is to reduce the degree of bainitic transformation.

The presence of solute depleted regions in the heterogeneous samples is expected to locally promote the formation of bainite at temperatures which are above  $B_s$  for the homogeneous samples. This explains why at relatively high temperatures, the degree of transformation is lower in the homogenised samples. Metallography (Figs. 4.1 and 4.9) provides clues as to why the situation reverses when transformation is carried out at higher undercoolings below  $B_s$ , with the homogeneous samples undergoing a higher degree of transformation at any given temperature. It is evident that in the homogeneous samples, the bainite nucleates uniformly at all locations, whereas in the heterogeneous specimens the substitutional-solute enriched regions do not transform at all. Furthermore, the untransformed bands in the latter specimens do not serve as sinks for the carbon that partitions from the bainitic ferrite, since most of that carbon is likely to be trapped in regions between the bainite subunits. If the bands could act as sinks for carbon then this would permit further transformation in the substitutional-solute depleted regions. To explore these qualitative arguments in more detail, a computer model was designed to simulate the development of bainitic transformation in chemically heterogeneous steels.

#### *4.2.2 Transformation Model*

To model the transformation behaviour, the heterogeneous steel was represented as a composite of  $N$  slices of equal thickness (Fig. 4.13). Each slice, identified by a subscript  $i$ , was assigned a different chemical composition consistent with the experimental measurements of composition as a function of distance. The composition within the slice was set to be uniform. The mean composition of all the slices was identical to the mean composition of the as-received 300M steel.

The calculation was carried out in stages, with each stage identified by the subscript  $j$ . For each value of  $j$  (i.e., at each stage of the calculation), the volume fraction of bainite in each slice was incremented by a small fraction  $\Delta V$ , provided transformation is thermodynamically feasible in that slice. Since bainite has to nucleate at the beginning of transformation in any slice, the condition for detectable nucleation of bainite is given by simultaneously satisfying the equations:

$$\Delta G^{\gamma-\gamma+\alpha} \leq \Delta G_N \quad (4.4)$$

and

$$\Delta G^{\gamma-\alpha} \leq 0 \text{ J mol}^{-1} \quad (4.5)$$

where  $\Delta G^{\gamma-\gamma+\alpha}$  is the free energy change accompanying the nucleation of a very small amount of bainitic ferrite, and  $\Delta G_N$  is the minimum free energy change that is necessary in order to obtain a detectable rate of nucleation<sup>[15,18]</sup>; the function  $\Delta G_N$  has been defined as:

$$\Delta G_N = 3.25175(T - 273.15) - 2183 \text{ J mol}^{-1} \quad (4.6)$$

where the units of temperature are in Kelvin.

Equation 4.4 therefore defines the thermodynamic condition that has to be satisfied in order to obtain a detectable nucleation rate for bainite, and Eq. 4.5 defines the thermodynamic condition for growth to be feasible, i.e., that the driving force for diffusionless transformation to bainitic ferrite  $\Delta G^{\gamma-\alpha}$  should exceed the stored energy of bainite. Simultaneous solution of the two equations gives the local bainite-start temperature for a given slice,  $B_s^i$ . Hence, at the beginning of transformation in a given slice, the calculated bainite-start temperature must be above the isothermal transformation temperature  $T_i$  if that slice is to transform at all:

$$B_s^i > T_i \quad (4.7)$$

Once the nucleation condition has been satisfied, the rules governing subsequent transformation can be less restrictive since only the growth condition (Eq. 4.5) needs to be satisfied. The formation of bainite involves diffusionless growth, but the excess carbon in the bainitic ferrite is immediately afterwards partitioned into the residual